BIOCHEMISTRY
including biophysical chemistry & molecular biology

Article

pubs.acs.org/biochemistry

Breaking the Proximal Fe^{II}–N_{His} Bond in Heme Proteins through Local Structural Tension: Lessons from the Heme *b* Proteins Nitrophorin 4, Nitrophorin 7, and Related Site-Directed Mutant Proteins

Chunmao He,[†] Saburo Neya,[‡] and Markus Knipp*[,†]

[†]Max-Planck-Institut für Bioanorganische Chemie, Stiftstrasse 34-36, D-45470 Mülheim an der Ruhr, Germany

[‡]Department of Physical Chemistry, Graduate School of Pharmaceutical Sciences, Chiba University, Image-Yayoi, Chiba 263-8522, Japan

Supporting Information

ABSTRACT: The factors leading to the breakage of the proximal iron–histidine bond in the ferroheme protein soluble guanylate cyclase (sGC) are still a matter of debate. This event is a key mechanism in the sensing of NO that leads to the production of the second-messenger molecule cGMP. Surprisingly, in the heme protein nitrophorin 7 (NP7), we noticed by UV–vis absorbance spectroscopy and resonance Raman spectroscopy that heme reduction leads to a loss of the proximal histidine coordination, which is not observed for the other isoproteins (NP1–4). Structural considerations led to the generation and spectroscopic investigation of site-directed mutants NP7(E27V), NP7(E27Q), NP4(D70A), and NP2(V24E). Spectroscopic investigation of these proteins shows that the spatial arrangement of residues Glu27, Phe43, and His60 in the proximal heme pocket of NP7 is the reason for the weakened Fe^{II}–His60 bond through steric demand. Spectroscopic investigation of the sample of NP7 reconstituted with 2,4-dimethyldeuterohemin ("symmetric heme") demonstrated that the heme vinyl substituents are also responsible. Whereas the breaking of the iron–histidine bond is rarely seen among unliganded ferroheme proteins, the breakage of the Fe^{II}–His bond upon binding of NO to the sixth coordination site is sometimes observed because of the negative *trans* effect of NO. However, it is still rare among the heme proteins, which is in contrast to the case for *trans* liganded nitrosyl model hemes. Thus, the question of which factors determine the Fe^{II}–His bond labilization in proteins arises. Surprisingly, mutant NP2(V24E) turned out to be particularly similar in behavior to sGC; i.e., the Fe^{II}–His bond is sensitive to breakage upon NO binding, whereas the unliganded form binds the proximal His at neutral pH. To the best of our knowledge, NP2(V24E) is the first example in which the ability to use the His-on ↔ His-off switch was engineered into a heme protein by site-directed mutagenesis other than the proximal His itself. Steric tension is, therefore, introduced as a potential structural determinant for proximal Fe^{II}–His bond breakage in heme proteins.

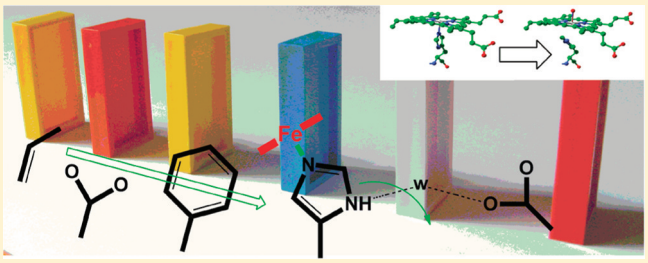

Nitrophorins (NPs) comprise a unique class of ferriheme proteins originating from the blood-feeding insect *Rhodnius prolixus*. The biological function of the NPs is the storage, transport, and delivery of NO from the insect to the host tissue, where NO acts as a vasodilator and blood-coagulation inhibitor.[2] The reactive molecule NO (in vivo, $t_{1/2} \approx 100$ ms)[3] is preserved through coordination to the heme iron inside the insect saliva. The protein experiences a significant pH change when subjected to the acidic pH of the saliva (between pH 5 and 6)[4] versus that of the blood plasma (~7.4); consequently, the affinity for NO is decreased, so that NO release occurs in the host tissue.

In NPs, the heme cofactor is located inside an eight-stranded β-barrel, which is an unusual case for a heme protein.[5] The protein fold has been classified as a lipocalin type of fold, which is a very common fold in the proteome. It is typically found in proteins that bind lipophilic molecules. The heme iron is coordinated by a His residue where the sixth coordination site is open for coordination of various small ligands.[6]

In contrast to other ferriheme proteins, i.e., met-myoglobin (metMb), which are reduced by excess NO (the so-called "autoreduction"),[7] in NPs the Fe^{III} state is stabilized by a number of carboxylate residues near the heme pocket[8] in combination with a ruffled heme geometry,[9] so that the reduction potential is established at, for example, −303 mV versus the SHE at pH 7.5 for NP1 compared to ~0 mV versus the SHE at pH 7.5 for Mb.[10] This is important for NP function because ferroheme–NO, i.e., $\{FeNO\}^7$ in the notation of Enemark and Feltham,[11] association constants are too large ($K_{eq} = 10^{13}$–10^{14} M^{-1})[8−10,12−14] to allow sufficient NO release under in vivo conditions.[15] In contrast, the NO association constants of ferriheme NPs, i.e., $\{FeNO\}^6$, are significantly smaller, for example, 4.0×10^6 M^{-1} for NP7 at pH 7.5.[14]

Received: July 12, 2011
Revised: August 24, 2011
Published: August 25, 2011

Although nitrophorins are ferriheme proteins, the Fe^{II} state came recently into focus when the Fe^{II}−CO derivative was used as a model for the $\{FeNO\}^6$ complex, for example, in FT-IR and laser flash photolysis experiments.[16,17] Previously, the crystal structures of several NP4[Fe^{II}] derivatives were reported.[18] Furthermore, the determination of $Fe^{III} \rightarrow Fe^{II}$ reduction potentials by spectroelectrochemistry was extensively used for the characterization of NP structure−function relationships.[8−10,12−14] Moreover, the Fe^{II} state was proposed as an intermediate in the reduction of the NP iron center with several low-molecular weight thiols.[19] Therefore, deeper investigation of the properties of ferroheme nitrophorins is required.

In a broader context, the production, handling, and sensing of NO in vertebrates are eminently associated with heme proteins. Thus, the NO production is performed at the heme-containing active site of nitric oxide synthases (NOSs).[20] This cytochrome P450 type of enzyme acts in the higher oxidation states of iron, so that the product NO is bound to the ferriheme protein. In contrast, the sensing of NO by soluble guanylate cyclase (sGC) is performed in the Fe^{II} oxidation state.[21] Recently, the involvement of other heme proteins, in particular the globins, with respect to NO signaling and the associated handling of this radical was brought to attention.[22,23] The members of this class of heme proteins are typically in the Fe^{II} oxidation state, which then forms very stable complexes with NO. However, recently, the partial existence of met-globins, in particular met-hemoglobin (metHb), in conjunction with the NO metabolism is discussed. Altogether, comparison of the properties of heme proteins improves our understanding of the structure−function relationships. At present, a systematic investigation of the ferroheme NPs is missing. Therefore, this study was initiated with the aim of investigating the properties of ferroheme nitrophorins NP4 and NP7.

EXPERIMETAL PROCEDURES

Materials. Stock solutions of $Na_2S_2O_4$ were prepared freshly before use. The effective concentration of $Na_2S_2O_4$ was determined through reduction of $[Fe(CN)_6]^{3-}$ in deaerated water (ε_{420} = 1026 M^{-1} cm^{-1}).[24] All reagents were of the highest grade commercially available and used as received. Catalase and glucose oxidase (both from *Aspergillus niger*) were bought from Serva. *S*-[^{15}N]Nitrosoglutathione ($GS^{15}NO$) was prepared as previously described.[25,26] Iron 2,4-dimethyldeuteroporphyrin ("symmetric heme") was prepared as previously described.[27]

Most experiments were performed under strictly anaerobic conditions inside an anaerobic tent (Coy Ltd.) with an atmosphere consisting of 98% N_2 and 2% H_2 in the presence of Pd catalysts. All solutions were rendered essentially O_2 free by three freeze−pump−thaw cycles performed on a vacuum line ($p < 0.5 \times 10^{-4}$ mbar). In addition, after the solutions were brought to the anaerobic environment, they were supplemented with 100 mM D-glucose, 0.1 mg/mL glucose oxidase, and 300 units/mL catalase.[28]

Molecular Biology. For the expression of the mutant protein NP4(D70A), plasmid pNP4(D70A)^{Kan} was generated by the QuikChange mutagenesis method[29] from the *wt* NP4 expression plasmid[12] using *Pfu* DNA polymerase (Stratagene). The following primers were used: 5′-TGG TAC GTG ACA GAT TAC CTA AAC TTG GAA CCT GAC GAC GTT CCA-3′ and 5′-TGG AAC GTC GTC AGG TTC CAA GTT TAG GTA ATC TGT CAC GTA CCA-3′ (the sites of mutation are underlined). The correctness of the coding regions of all expression plasmids was confirmed via DNA sequencing.

Production of Recombinant Proteins. Prior to expression, plasmids were transformed into *Escherichia coli* strain BL21(DE3) (Novagen). NP4 and NP4(D70A) were expressed, reconstituted, and purified as described previously for NP4.[13] The other proteins were reconstituted by a stepwise heme insertion described for the preparation of NP7.[30,31] The protein preparations were judged by sodium dodecyl sulfate−polyacrylamide gel electrophoresis to be >90% pure. Proteins were also subjected to MALDI MS to confirm the correct molecular masses, including two Cys−Cys disulfide bonds: calcd for $[NP4 + H]^+$ 20264 Da, observed 20,296 Da; calcd for $[NP4(D70A) + H]^+$ 20220 Da, observed 20225 Da; calcd for $[NP7 + H]^+$ 20969 Da, observed 21002 Da; calcd for $[NP7(E27Q) + H]^+$ 20969 Da, observed 20975 Da; calcd for $[NP7(E27V) + H]^+$ 20939 Da, observed 20939 Da; calcd for $[NP2(V24E) + H]^+$ 20080 Da, observed 20070 Da. Proteins were kept at −20 °C in 200 mM NaOAc/HOAc and 10% (v/v) glycerol (pH 5.0) until use.

Absorption Spectroscopy. A Cary-50 spectrophotometer (Varian, Inc.) equipped with an opto coupler (Varian, Inc.) was placed outside the glovebox. The light beam was led inside and outside the glovebox by glass fibers (Ocean Optics) that were connected to a cuvette holder (Ocean Optics). Thus, absorbance spectra were recorded under O_2-free conditions in quartz cuvettes. pH titrations were performed in a 3 mL cuvette with a small pH glass electrode inserted into the solution such that the electrode did not cross the beam. pH titrations were performed with dilute HOAc or KOH solutions, and the actual pH was read upon mixing.

Resonance Raman Spectroscopy. To largely deplete the protein solution of O_2, the solvent was exchanged with the respective anaerobic buffer inside the glovebox and the protein concentration was adjusted to ∼25 μM. The ferroheme species was prepared by careful titration with stoichiometric amounts of a freshly prepared $Na_2S_2O_4$ solution. To form the NO complexes, the protein solution was thereafter titrated with a DEA/NO solution in 10 mM NaOH under photometric control. The ^{15}NO complexes were prepared by incubation with $GS^{15}NO$ in the presence of catalytic amounts of CuCl.[14,a] Ambient-temperature measurements were performed in a rotating cylindrical quartz cuvette (5.5 cm diameter, ∼3 mL volume), which was closed with rubber stoppers to prevent reoxidation. The integrity of the samples was monitored by the recoding of a second spectrum right after the original measurement. In the case of a significant difference, i.e., indicating oxidation, the spectra were discarded. RR spectra were recorded with a scanning double monochromatic. The excitation line at 413.1 nm was provided by a coherent K-2 Kr^+ ion laser, and the sample was rotated throughout the measurement to minimize radiation damage.

RESULTS

Reduction of the Heme Iron of Nitrophorins with $Na_2S_2O_4$. We have shown elsewhere that the incubation of NP4 and NP7 with excess $Na_2S_2O_4$, which is a common method for the formation of ferroheme proteins, leads to protein damage because of the reduction of the two Cys−Cys disulfides contained in the protein structure.[32] Furthermore, it was previously reported that the reduced NP4 was somehow unstable,[18,33] and we had shown that this results from the presence of atmospheric O_2.[34] As a consequence, ferroheme

NPs in this study were exclusively prepared by the careful titration with stoichiometric amounts of $Na_2S_2O_4$. The preparation was monitored by UV−vis absorption spectroscopy, and the reduced compounds were handled under strictly anaerobic conditions thereafter. As one can see from Figure 1A,

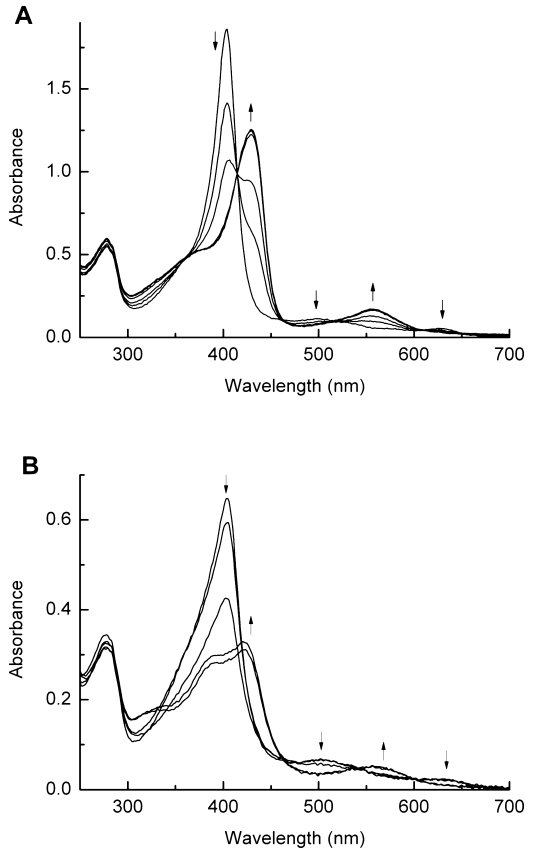

Figure 1. Reduction of (A) 12 μM NP4 and (B) 8.6 μM NP7 with $Na_2S_2O_4$ in 100 mM MOPS/NaOH and 50 mM NaCl (pH 7.5) monitored by UV−vis absorption spectroscopy under anaerobic conditions.

the titration of NP4 with $Na_2S_2O_4$ under anaerobic conditions leads to a shift of the Soret band absorption maximum from 403 to 429 nm and the appearance of a broad Q-band at ∼557 nm, which is in good agreement with the previously reported data.[18] The spectral conversion is accompanied by good isosbestic behavior. In contrast, when the same experiment was performed with NP7 (see Figure 1B), two Soret band absorption maxima were found at 422 and 388 nm and a broad Q-band with a maximum at ∼560 nm was obtained. Furthermore, the titration does not show isosbestic behavior, thus indicating the formation of more than one heme species.

Other ferroheme proteins with a proximal His, for example, sperm whale deoxyMb, exhibit a similarly blue-shifted Soret band when His coordination is lost[35,36] (compare in Table 1). This can happen particularly under acidic conditions; for example, at pH <4, deoxyMb undergoes a loss of secondary structure, which leads to a weakening of the Fe^{II}−His bond causing a Soret band shift from 434 to 383 nm. At this low pH, protonation of the proximal His N^{τ} atom competes with Fe^{II} coordination. However, in the case of NP7, the pH of 7.5 (Figure 1B) largely exceeds the typical pK_a of the His side chain (∼6.0), and therefore, the reaction upon reduction may be

Scheme 1. Effect of One-Electron Reduction on the Coordination Environment of the Heme Iron in NP7

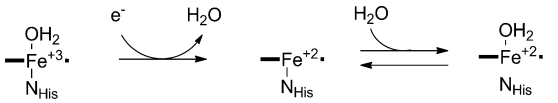

better described by an equilibrium depicted in Scheme 1. Furthermore, in contrast to Mb, of which the Soret band maximum at low pH is similar to the spectrum of free reduced hemin with absorbance maxima at 383 and ∼581 nm (see Figure S2 of the Supporting Information), the absorption spectrum of NP7 at neutral pH is significantly different, which strongly indicates the integrity of the protein−heme complex.

Spectroscopic Characterization of NP4- and NP7-[Fe^{II}]. For the detailed elucidation of the coordination sphere of the single NP4[Fe^{II}] species and the two (or more) NP7[Fe^{II}] species observed in the UV−vis spectrum (Figure 1), RR spectra in the high-frequency range (1200−1650 cm^{-1}) were recorded at ambient temperature where the chromophore was excited into the Soret band at 413.1 nm. The resulting spectra are displayed in Figure 2 together with those of the

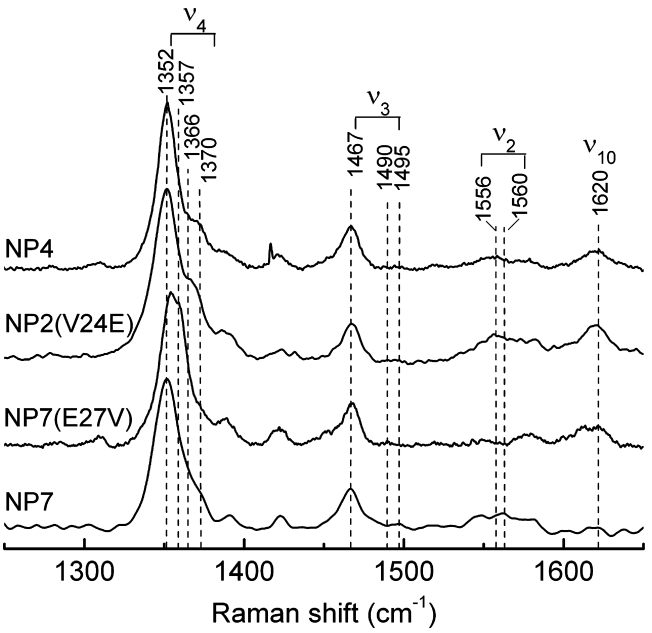

Figure 2. High-frequency region of the RR spectra of ∼25 μM NP4[Fe^{II}], NP2(V24E)[Fe^{II}], NP7(E27V)[Fe^{II}], and NP7[Fe^{II}] in 100 mM MOPS/NaOH and 50 mM NaCl (pH 7.5) recorded at ambient temperature (λ_{ex} = 413.1 nm).

mutant proteins NP2(V24E)[Fe^{II}] and NP7(E27V)[Fe^{II}], which will be discussed later. The high-frequency region of the RR spectra of heme proteins includes information about the Fe coordination sphere and the spin state.[37,38] In Table 1, the Raman shift frequencies of selected resonances with diagnostic potential for the assignment of the oxidation state and spin state are summarized in comparison with those of several other ferroheme protein representatives.

The most prominent core-size marker band in the high-frequency region of the RR spectra of heme proteins is the oxidation state marker ν_4 that indicates the presence of a ferric (1370−1375 cm^{-1}) or ferrous iron oxidation state (1350−1375 cm^{-1}).[37,39−42] In NP4, the ν_4 of 1352 cm^{-1} clearly confirms the +2 oxidation state of the iron, although the appearance of a

dx.doi.org/10.1021/bi201073t | Biochemistry 2011, 50, 8559−8575

Table 1. Comparison of the Electronic Absorption Maxima and Heme Raman Shifts of Ferrous Nitrophorins and Other Ferrous Heme Proteins with Proximal His Ligands Recorded at Room Temperature

		absorption maximum (nm)			Raman shift (cm^{-1})					
Fe^{II} protein	pH	λ_{Soret}	λ_{β}	λ_{α}	ν_4	ν_3	ν_2	Fe^{II} axial ligands	coordination number and spin state[a]	ref
NP1	7.5				1353	1467		His	5cHS	45
NP2(V24E)	7.5	425		556	1352	1467	1556	His	5cHS	tw[b]
NP4	7.5	429		556	1352	1467	1556	His	5cHS	tw[b]
NP7	7.5	422		561	1352	1467	1560	His	5cHS	tw[b]
		388			1366	1495		H_2O	5cHS	
NP7	5.5	386		574	1366	1491	1555	H_2O	5cHS	tw[b]
					1370	1504	1560	none	4cIS	
NP7	10.5	422	527	577	1355	1488	1576	His/OH^-	6cLS	tw[b]
NP7(E27V)	7.5	427		560	1354	1468		His	5cHS	tw[b]
					1357	1490		His/OH^-	6cLS	
NP7(E27Q)	7.5	422		560				His	5cHS	tw[b]
		392						H_2O	5cHS	
$NP7_{sym}$	7.5	410		~545				His	5cHS	tw[b]
Mb[c]	6.9	435		555	1354	1472	1563	His	5cHS	35
Mb[c]	3.8	426		546	1357	1495	1565	H_2O	5cHS	35
		383			1371	1504		no	4cIS	
cyt c'[d]	7.0				1352	1469	1577	His	5cHS	49
cyt c'[d]	12.0				1358	1488	1592	His/Lys	6cLS	49
cyt c'[e]	12.4				1360	1494	1585	His/Lys	6cLS	48
hHO-1(H25A)[f]	7.4	426	551	587	1357	1471	1562	?	5cHS	47
					1368	1500		none	4cIS	
*Vc*H-NOX[g]	7.5	429	568		1354	1471	1561	His	5cHS	108
*Tt*H-NOX[h]	7.5	431	565		1354	1471	1575	His	5cHS	108
NPAS2 bHLH-PAS-A[i]	8.0	426	530	559	1359	1471	1555		5cHS	109
						1493	1582		6cLS	
HRI[j]	8.0	426	531	560				His/?	6cLS	110
reduced hemin	7.5	381		~581						tw[b]

[a]HS, high-spin; LS, low-spin; IS, intermediate-spin. [b]This work. [c]From sperm whale. [d]From *Chromatium vinosum*. [e]From *Rhodospirillum rubrum*. [f]H25A mutant of human liver heme oxygenase. [g]H-NOX domain from *Vibrio cholerae*. [h]H-NOX domain from *Thermoaerobacter tengcongensis*. [i]N-Terminal basic helix−loop−helix (bHLH) motif of the first PAS (PAS-A) domain of NPAS2. [j]Heme-regulated eukaryotic initiator factor 2α kinase.

small shoulder at ~1370 cm^{-1} may indicate the presence of a small amount of ferric protein, i.e., developing from air oxidation during the recording of the spectra. Another important feature seen in Figure 2 is the so-called spin-state marker ν_3 that appears at 1467 cm^{-1}. The ν_3 porphyrin skeletal mode is well established to be sensitive to the heme core size, which changes with the spin state of the iron depending on the oxidation state, i.e., 1460−1470 cm^{-1} for a 5cHS Fe^{II} and 1490−1510 cm^{-1} for a 5cLS or 6cLS Fe^{II},[41−43] thus assigning NP4[Fe^{II}] as a His-liganded 5cHS. Comparison with the spectral features of deoxyMb also shows that the ν_2 and ν_{10} bands at 1556 and 1620 cm^{-1}, respectively, further support this assignment.[35,36,44] This is in contrast to the previous report about the NP4[Fe^{II}] X-ray structure at pH 7.5 [Protein Data Bank (PDB) entry 1YWD] where electron density was found on the distal site of the heme iron that was modeled as an O atom, i.e., water.[18] However, the release of water from the heme is typical upon reduction of Fe^{III} to Fe^{II} as was shown for many heme proteins, including NP1[Fe^{II}][45] (compare in Table 1).

Also in the case of NP7[Fe^{II}], the oxidation state marker ν_4 at 1352 cm^{-1} is well in the range of a ferrous heme; however, significant broadening of the band is noticed (Figure 2). This may be a consequence of the appearance of two or more different coordination environments on the iron, which is inferred already from the UV−vis spectrum (Figure 1). The ν_3 of 1467 cm^{-1}, like that for NP4[Fe^{II}], reflects a major fraction of His-liganded NP7[Fe^{II}]. Similar to the NP4 sample, a small fraction of reoxidized heme can be attributed to the shoulder at ~1373 cm^{-1}[146] (λ_{Soret} = 404 nm).[30] However, an additional shoulder at ~1366 cm^{-1}, in agreement with the absorption spectrum, can be attributed to the presence of another ferroheme species, i.e., 5c $Fe^{II}-OH_2$. This was also observed for deoxyMb at pH 3.8 where protonation of the proximal His leads to the breakage of the $Fe-N_{His}$ bond.[35,36]

It was observed by absorption spectroscopy that a decrease in pH causes the Soret band ratio to shift toward the 386 nm species (see below). Figure 3 displays the RR spectrum at pH 4.0 where the absorption spectrum exhibits only the Soret band at 386 nm. In some cases, the ν_{Fe-His} stretching mode was observed at ~220 cm^{-1}, which is diagnostic for the presence of the Fe−His bond.[35,41,47] However, extensive background Raleigh scattering sometimes does not allow the observation of this very weak mode,[45] which is unfortunately also the case for NP4 and NP7. Nevertheless, the loss of the $Fe-N_{His}$ bond is indicated by the disappearance of the ν_4 band at 1352 cm^{-1}. Instead, a broad ν_4 band with a maximum at 1370 cm^{-1} is obtained (see below). At the same time, the broadening of ν_4 can be attributed to an underlying species at 1366 cm^{-1} that was also seen at pH 7.5 (see above), which agrees well with the existence of the water-on complex. This is further confirmed by the ν_3 of 1491 cm^{-1} and the ν_{10} of 1635 cm^{-1}. The appearance of the strong ν_4 at 1370 cm^{-1} may indicate a ferric heme.

dx.doi.org/10.1021/bi201073t | *Biochemistry* 2011, 50, 8559−8575

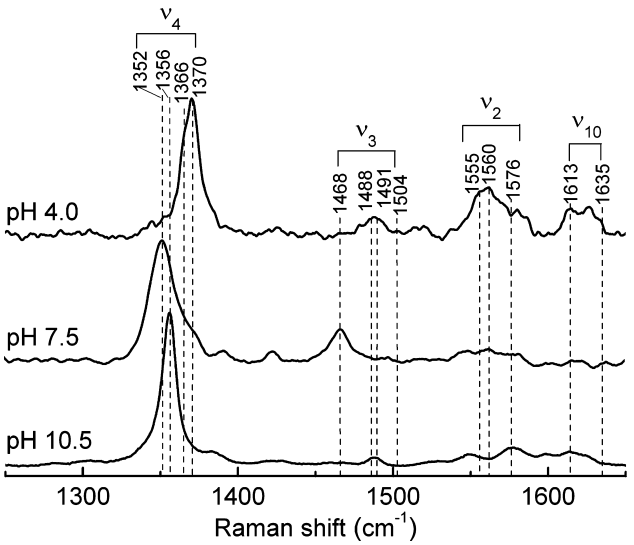

Figure 3. High-frequency range of the RR spectra (λ_{ex} = 413.1 nm) of NP7[Fe^{II}] at pH 4.0 (100 mM NaOAc/HOAc), pH 7.5 (100 mM MOPS/NaOH), and pH 10.5 (100 mM $NaHCO_3$/NaOH) recorded at ambient temperature.

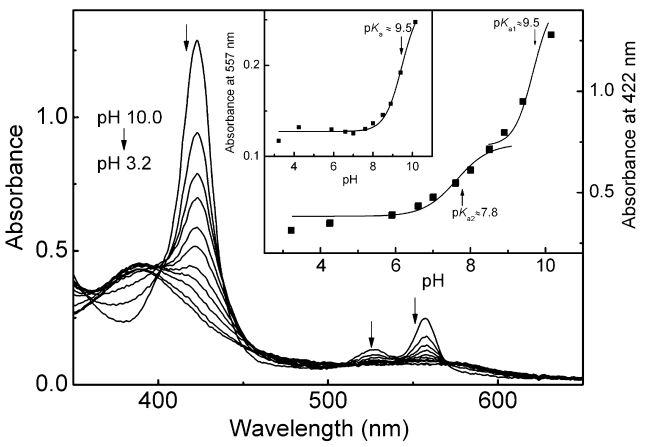

Figure 4. pH titration of NP7[Fe^{II}] monitored by UV−vis spectroscopy. The insets show the plots of the absorbancies at 422 and 557 nm versus pH.

However, oxidation can be ruled out on the basis of the absorption spectrum recorded after the RR measurement (data not shown). To interpret the spectrum, the novel ν_3 = 1504 cm^{-1} band has to be taken into account; by analogy to deoxyMb and the H25A mutant of hHO-1, it can be attributed to the presence of a 4c intermediate-spin (4cIS) ferrous heme.[47]

In addition to the low-pH sample, RR spectra of NP7[Fe^{II}] at pH 10.5 were also recorded (Figure 3). Inspection of core marker bands ν_4, ν_3, and ν_2 at 1356, 1488, and 1576 cm^{-1}, respectively, confirms the formation of a 6cLS Fe^{II} complex, which is well in agreement with the corresponding absorption spectrum (see below). In the case of σ-type interacting Fe^{II} ligands, the ν_3 and ν_4 bands typically appear at lower frequencies compared to π-backbonding ligands (ν_3 = 1494−1510 cm^{-1}; ν_4 = 1360−1372 cm^{-1}).[48] Many heme proteins contain a potential distal ligand; for example, in cyt *c*′, a Lys coordinates as a sixth ligand at elevated pH (so-called type n ferrocytochrome *c*′), whereas under moderate-pH conditions, the iron remains 5c (so-called type a ferrocytochrome *c*′).[48,49] In contrast, the distal pocket of NPs does not provide a residue with the ability to coordinate to the heme; thus, it can be concluded that an N_{His}−Fe^{II}−OH^- hydroxo complex is formed at elevated pH.

pH Titration of NP7[Fe^{II}]. The preceding experimental information was used to perform a pH titration on NP7[Fe^{II}] monitored by absorption spectroscopy. The experiment was conducted between pH 10.0 and 3.8, and the resulting spectra are depicted in Figure 4. Within these pH borders, the changes were fully reversible, which indicates the integrity of the protein. The hydroxo complex shows a strong Soret band absorption at 422 nm and the appearance of two sharp Q-bands at 557 nm (α-band) and 527 nm (β-band), which is characteristic for LS heme complexes. The plot of the Soret band absorption maximum versus pH exhibits two major transitions where the plot of the α-band absorbance versus pH exhibits only a single transition. Because this spectral change is attributed to the disappearance of the LS complex, i.e., N_{His}−Fe^{II}−OH^- + H^+ ⇆ N_{His}−Fe^{II} + H_2O, when the pH is decreased, the plot is used to determine the pK_a of the first transition (i.e., pK_{a1} ≈ 9.5). The second transition was then fit in the ΔA_{422} versus pH plot, yielding a pK_{a2} of ≈7.8. This process is fully reversible within the pH boundaries applied.

The pH dependence of the axial heme coordination in NP7 is summarized in Scheme 2.

Scheme 2. pH Dependence of the Heme Coordination in NP7[Fe^{II}]

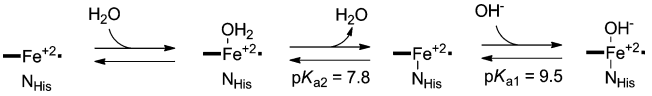

Absorption Spectra of Related Mutant Proteins. Mutant proteins NP7(E27V), NP7(E27Q), and NP2(V24E) were previously produced and their ferric oxidation states partly characterized.[31,50] Glu27 resembles the position of Val24 in NP2 and -3 or Val25 in NP1 and -4 and has a subtle influence on the heme properties. Thus, the E27V mutation in NP7 increases its level of similarity to *wt* NP1−4, whereas the V24E mutation in NP2 increases its level of similarity to *wt* NP7. NP7(E27Q) was created as a charge-depleted mutant of *wt* NP7. In addition, a novel mutant NP4(D70A) was engineered and for the first time recombinantly expressed.

Upon reduction of NP4(D70A), NP2(V24E), and NP7(E27V) with stoichiometric amounts of $Na_2S_2O_4$ under anaerobic conditions, isosbestic spectral change similar to NP4 was observed (data not shown). Figure 5 displays the resulting absorption spectra of NP4(D70A)[Fe^{II}], NP2(V24E)-[Fe^{II}], NP7(E27V)[Fe^{II}], and NP7(E27Q)[Fe^{II}] in comparison to those of *wt* NP4[Fe^{II}] and *wt* NP7[Fe^{II}] at pH 7.5. In summary, among this set of proteins, NP7(E27Q)[Fe^{II}] is the only protein that exhibits a Soret band splitting comparable to that of *wt* NP7[Fe^{II}], though the high-energy band maximum is shifted ∼4 nm toward the red. In contrast, the NP7(E27V)-[Fe^{II}] mutant not only lacks the high-energy Soret band but also shifts the low-energy Soret band maximum ∼5 nm to the red. The Q-band maxima of all NP7 types of proteins are shifted to the blue by 6−8 nm. The Soret band maximum is comparable to the 427 nm value of NP7(E27V), though it varies between 425 and 429 nm. Thus, these spectroscopic data fit well to the previous proposal that the presence of Glu27 is crucial for the special functionality of NP7; however, Glu27 can

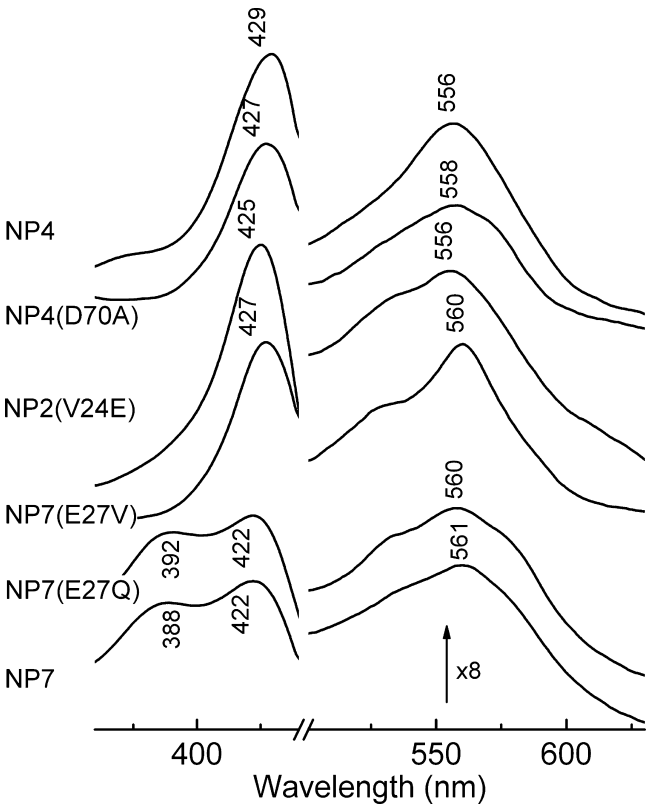

Figure 5. Comparison of the UV−vis absorption spectra of the Soret band and Q-band region of NP4[Fe^{II}], NP4(D70A)[Fe^{II}], NP2(V24E)[Fe^{II}], NP7(E27V)[Fe^{II}], NP7(E27Q)[Fe^{II}], and NP7[Fe^{II}] in 100 mM MOPS/NaOH and 50 mM NaCl (pH 7.5).

be substituted with Gln without a significant spectral change, indicating that the steric effect of the residue is more important than the charge. Nevertheless, the preparation of NP7(E27Q) yields only small amounts of protein and tends to precipitate at elevated concentrations, indicating that the charge of Glu27, though not crucial for the properties of the heme environment, is essential for protein folding.[31] However, comparison of the protein aromate absorbance at 280 nm with the Soret band absorbance indicates a filling of NP7(E27Q) comparable to that of the *wt*.

Resonance Raman Spectra of Related Mutant Proteins. The instability of most of the mutants also does not allow the recording of RR spectra, which requires relatively high protein concentrations. However, as one can see from Figure 2, NP7(E27V)[Fe^{II}] and NP2(V24E)[Fe^{II}] behave much like *wt* NP4[Fe^{II}] and NP7[Fe^{II}], and the respective Raman shifts are listed in Table 1. Overall, all spectra look very similar, indicating that the major species observed is the 5c His-on species, a finding supported well by the absorption spectra. However, the ν_4 band of NP7(E27V)[Fe^{II}] is rather broad, and the shoulder at 1357 cm^{-1} can be assigned to a significant fraction of the hydroxo species, similar to the spectrum of NP7[Fe^{II}] at higher pH values (Figure 3). This is supported by the appearance of the weak ν_3 band at 1490 cm^{-1}. Furthermore, like in NP4[Fe^{II}] and NP7[Fe^{II}], the shoulder at ~1370 cm^{-1} is attributed to a minor fraction of oxidized material.

Absorption Spectra of NP4- and NP7[Fe^{II}−NO] and Corresponding Mutant Proteins. The previous studies were accompanied by the examination of the ferroheme nitrosyl complexes. Fe^{II} porphyrins form very tight complexes with NO where NO exhibits a strong negative *trans* effect on the proximal ligand[51,52] that makes it hard to prepare good synthetic models of 6c {FeNO}^{7} complexes,[53] although few such complexes were reported.[54,55] In contrast, in proteins the His ligation is typically preserved upon NO binding. However, a number of ferroheme proteins, in particular those that are involved in NO signaling, lose His coordination upon NO binding. Prominent examples are the CooA from *Rhodospirillum rubrum*,[56] mammalian sGC,[57] and the neuronal PAS protein 2.[58] However, the structural factors that determine the weakening or strengthening of the *trans* bond are not clear, although it is important to understand the structure−function relationships of such proteins, not at least because of the physiological importance and pharmacological potential associated with sGC.[59]

In the case of NP7[Fe^{II}], because of the already weakened N_{His}−Fe^{II} bond, the loss of the coordination upon NO binding is expected. It was previously reported that NP4[Fe^{II}−NO] is a His-on species.[18] In marked contrast, the absorption spectrum of NP7[Fe^{II}−NO] displayed in Figure 6 indicates that this form

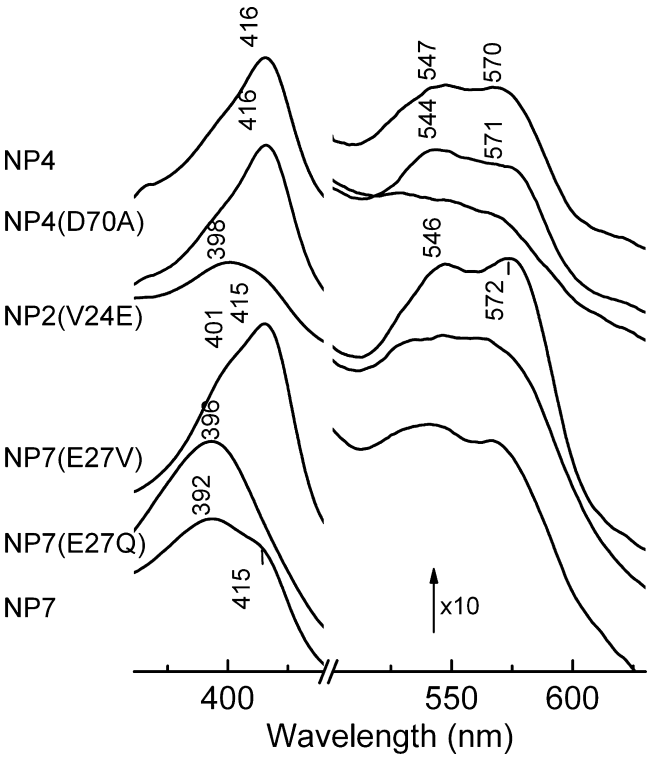

Figure 6. UV−vis absorption spectra of *wt* NP4[Fe^{II}−NO] and *wt* NP7[Fe^{II}−NO] and corresponding mutant proteins in 100 mM MOPS/NaOH and 50 mM NaCl (pH 7.5).

comprises mostly a 5c species (392 nm), although a significant amount of the Soret band absorption from the His-on species can be seen (~415 nm). Interestingly, the E27Q mutation in NP7 leads to only the His-off species. On the other hand, insertion of Val27 into NP7 reverses this effect, and the absorption spectrum displays mainly the His-on species, though a small contribution is assigned to the His-off species.

In contrast to the mutations of Glu27 in NP7, mutation of Asp70, i.e., NP4(D70A), does not alter the behavior of NP4, which agrees well with the previous finding for NP4(D70A)-[Fe^{II}] (see above). To our surprise, though, NP2(V24E)[Fe^{II}−NO] completely loses the N_{His}−Fe^{II} coordination.

dx.doi.org/10.1021/bi201073t | *Biochemistry* 2011, 50, 8559−8575

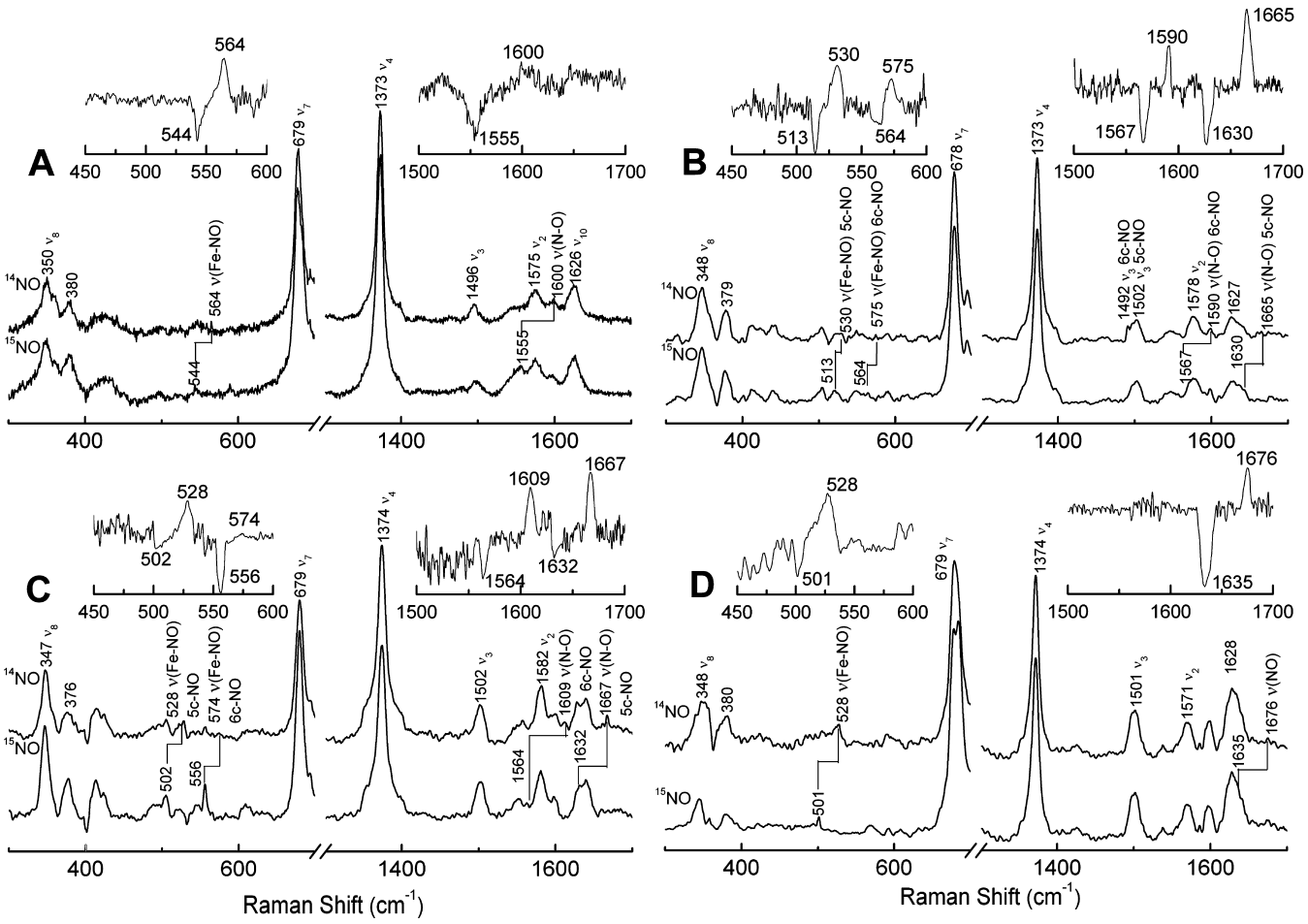

Figure 7. Comparison of the RR spectra of (A) NP4[Fe^{II}–NO], (B) NP7(E27V)[Fe^{II}–NO], (C) NP7[Fe^{II}–NO], and (D) NP2(V24E)[Fe^{II}–NO] in 100 mM MOPS/NaOH and 50 mM NaCl (pH 7.5) at ambient temperature (λ_{ex} = 413.1 nm).

Resonance Raman Spectra of NP4- and NP7[Fe^{II}–NO] and Corresponding Mutant Proteins. Similar to the previous assignment of the coordination state of the unliganded NPs, the absorption spectra were accompanied by the recording of RR spectra. For the unambiguous assignment of the ν_{Fe-NO} and ν_{N-O} stretch vibrations, samples with ^{14}NO and ^{15}NO were measured. The resulting RR spectra of NP4[Fe^{II}–NO], NP7[Fe^{II}–NO], NP2(V24E)[Fe^{II}–NO], and NP7(E27V)[Fe^{II}–NO] were recorded, and they are presented in Figure 7. The corresponding Raman shifts are summarized in Table 2 together with the corresponding data of relevant proteins from the literature.

The RR spectrum of NP4[Fe^{II}–NO] at pH 7.5 is depicted in Figure 7A. In the high-frequency region of the RR spectra, core-size marker bands, ν_4, ν_3, and ν_2 at 1373, 1496, and 1575 cm^{-1}, respectively, are consistent with those reported for 6c ferrous heme–NO complexes.[60−65] The Fe^{II}–NO stretching frequency is sensitive to heme coordination number, while a 5c heme–NO stretch typically falls between 510 and 530 cm^{-1}[66] and a 6c heme–NO stretch between 530 and 590 cm^{-1}.[55] The ν_{Fe-NO} for NP4[Fe^{II}–NO] is 564 cm^{-1} and shifts down to 544 cm^{-1} with ^{15}NO. NP4(D70A)[Fe^{II}–NO] also has a 6c heme as judged from the UV–vis absorption spectrum. The broad Soret band has a maximum at ~400 nm for NP7[Fe^{II}–NO] and NP7(E27Q)[Fe^{II}–NO] and is consistent with those reported for 5c ferrous heme–NO complexes.[56,64,67−69] This is further confirmed by the RR spectrum. The core-size marker bands (Figure 7C), ν_4, ν_3, and ν_2 at 1374, 1502, and 1582 cm^{-1}, respectively, identify NP7[Fe^{II}–NO] as a 5c ferrous heme–NO complex.[70,71] The ν_{Fe-NO} mode for NP7[Fe^{II}–NO] appears at 528 cm^{-1}, which is also very characteristic for a 5c ferrous heme–NO complex. As mentioned above, the UV–vis spectrum (Figure 6) indicates a small fraction of the 6c His-on species, the concentration of which is too small, compared to that of the 5c His-off species, to detect the corresponding Raman shift in the core-size marker bands. However, the much better resolved ν_{Fe-NO} and ν_{N-O} modes appear at 574 and 1609 cm^{-1}, respectively, which is confirmed by the spectrum of the ^{15}NO-labeled species.

NP7(E27V)[Fe^{II}–NO] has a Soret band maximum at 415 nm and a shoulder at 401 nm, which suggests the coexistence of 6c and 5c ferrous heme–NO complexes. This can be confirmed by the RR spectrum (Figure 7B): for the 6c NO complex, ν_3 = 1492 cm^{-1} and ν_{Fe-NO} = 550 cm^{-1}, and for the 5c NO complex, ν_3 = 1502 cm^{-1} and ν_{Fe-NO} = 530 cm^{-1}.

In contrast to the three previously reported proteins, NP2(V24E)[Fe^{II}–NO] did not exhibit any signature of the 6c His-on form in the UV–vis spectrum. Accordingly, the RR spectra provide only the ν_{Fe-NO} and ν_{N-O} modes at 528 and 1676 cm^{-1}, respectively, that correspond to the 5c His-off species (Figure 7D). The core-size marker bands all agree well with this interpretation.

Ferroheme NP7 Reconstituted with Symmetric Heme. A significant lack of symmetry in protoporphyrin IX

dx.doi.org/10.1021/bi201073t | Biochemistry 2011, 50, 8559–8575

Table 2. Comparison of the Absorption Maxima and Heme Raman Shifts of the Nitrosyl Complexes of Ferrous Nitrophorins with Those of the Nitrosyl Complexes of Other His-Liganded Ferrous Heme Proteins Recorded at Room Temperature

		absorption maximum (nm)			Raman shift (cm^{-1})					
protein	pH	λ_{Soret}	λ_{β}	λ_{α}	ν_4	ν_3	ν_2	ν_{Fe-N}	ν_{N-O}	ref
					6cNO[a]					
NP1	8.0	416							1611[b]	10
NP2(D1A)	7.5	414								8
NP4	7.5	416	547	570	1373	1496	1575	564	1600	tw[c]
NP4(D70A)	7.5	416	544	571						tw[c]
NP7(E27V)	7.5	415	546	572	1373	1496	1571	575	1590	tw[c]
NP7	7.5	415						574	1609	tw[c]
Mb[d]	7.4	421			1375	1500	1583	558	1613	60
Mb[e]	7.0							552	1612	93
Mb(H64L)[e]	7.0							563	1635	93
Mb(H64I)[e]	7.0							558	1638	93
Cygb[f]	8.0				1376	1502	1574	569	1604	61
Ngb[g]	8.0				1375	1498	1572	573	1600	61
FixLN[h]	7.8	420	546	578	1373	1498	1575	558		62
BjFixLH[i]	7.0					1498	1575	568	1634	63
AXCP[j]	8.9	415	540	575	1375	1504	1596	579	1624	64
RCCP[k]	7.0	414	540	570	1377	1506	1598	569	1625	65
*Tt*H-NOX[l]	7.5	420	545	575	1371	1496	1580	553	1655	108
					5cNO[m]					
NP2(V24E)	7.5	398			1374	1501	1571	528	1675	tw[c]
NP7	7.5	392	540	572	1373	1504	1583	528	1667	tw[c]
NP7(E27V)	7.5	401	546	572	1373	1502	1581	530	1665	tw[c]
NP7(E27Q)	7.5	396	540	572						tw[c]
$NP7_{sym}$	7.5	387	525	562						tw[c]
NP2(D1A/D29A)	5.5	398								8
	7.5	400[n]								8
NP2(D1A/D36A)	5.5	398								8
	7.5	400[o]								8
NP4(D30A)	5.5	407[o]								8
	7.5	404								8
sGC_2[p]	7.4	398	537	572	1375	1509	1584	525	1677	67, 68
*Vc*H-NOX[q]	7.5	398	537	572	1372	1505	1580	525	1677	108
CooA[r]	7.4	399	544	572	1376	1506	1582	523	1672	56
CLOCK PAS-A[s]	7.1	396	541	577	1374	1508	1588	525	1668	69
AXCP[j]	8.9	395	539	565	1373	1506	1592	526	1661	64
NPAS2 bHLH-PAS-A[t]	8.0	394			1376	1508	1584	523	1670	109
HRI[u]	8.0	398	538					524	1677	110

[a]Six-coordinate nitrosyl complexes, proximal His bound. [b]Determined by FT-IR spectroscopy. [c]This work. [d]From horse heart. [e]Recombinant human myoglobin. [f]Human cytoglobin. [g]Human neuroglobin. [h]FixLN, a membrane-bound protein from soil bacterium *Rhizobium meliloti*. [i]BjFixLH, the heme-binding domains of *Bradyhizobium japonicum* FixL. [j]AXCP, *Alcaligenes xylosoxidans* cytochrome *c*′, measured at 90 K. [k]RCCP, *Rhodobacter capsulatus* cytochrome *c*′. [l]H-NOX domain from *T. tengcongensis*. [m]Five-coordinate nitrosyl complexes. [n]Shoulder at ∼413 nm. [o]Shoulder at ∼415 nm. [p]From bovine lung. [q]H-NOX domain from *V. cholerae*. [r]CooA, CO oxidation activator protein from *R. rubrum*. [s]CLOCK PAS-A, mammalian circadian protein CLOCK. [t]N-Terminal basic helix−loop−helix (bHLH) motif of the first PAS (PAS-A) domain of NPAS2. [u]Heme-regulated eukaryotic initiator factor 2α kinase.

is achieved by the particular pattern of substituents at the aromatic core, as shown in Scheme 3. As a consequence, the cofactor can orient inside a protein heme pocket in two different orientations, **A** and **B**, a phenomenon that has been termed "heme rotational disorder" (see Scheme 3). Using NMR, it was shown that NP1 and -4 have no preference for one orientation (≈1:1 **A**:**B**) whereas NP2 and -3 exhibit a preference for the **B** orientation.[13,72−74,b] In contrast, using ^{1}H NMR and circular dichroism (CD) spectroscopy, NP7 was found to be the only member of the NP family that stabilizes the heme **A** orientation.[14,31] By use of the mutants NP7(E27V) and NP7(E27Q), which were also applied in this study, it was determined that Glu27 in NP7 is responsible for the formation of the **A** orientation. NP7 is the only NP that exhibits a Glu residue at this position where NP1−4 have a Val (see Figure S1 of the Supporting Information). Consequently, insertion of this residue into NP2, i.e., NP2(V24E), results in the **A** orientation.[31,50] An examination of the protein structure suggests that the steric demand of Glu27 causes repulsion of the cofactor.

To understand the extent to which the vinyl groups of the cofactor influence the steric interaction with the NPs, we reconstituted NP7 with symmetric heme. The absorbance spectrum of the complex is shown in Figure 8 together with the spectra of the ferroheme species and the Fe^{II}−NO complex. When compared to the native form, all species show absorbance spectra with their maxima shifted ∼10 nm to the

dx.doi.org/10.1021/bi201073t | *Biochemistry* 2011, 50, 8559−8575

Scheme 3. Heme *b* Nomenclature and Heme Orientation inside the Pocket of NP2[a]

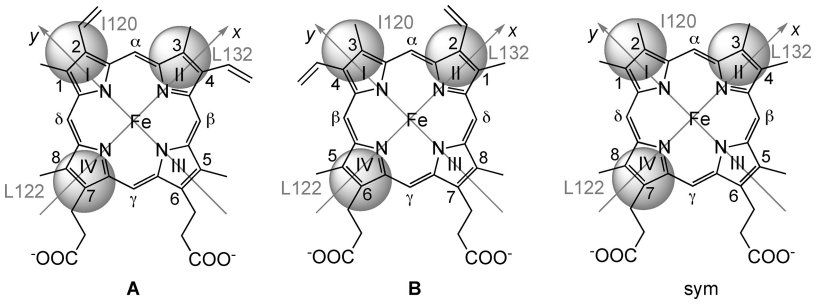

[a]The heme pocket of NP2 is indicated by the three circles corresponding to the positions of the three aliphatic side chains pointing from the top of the distal pocket onto the heme plane. The two possible heme orientations are indicated as **A** and **B**. The "symmetric heme" (2,4-dimethyldeuterohemin) used in this study is designated sym.

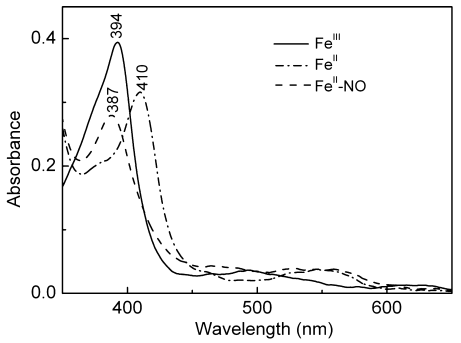

Figure 8. Absorption spectrum of NP7 reconstituted with symmetric heme in +3 and +2 iron oxidation states and of the ferroheme−nitrosyl complex. Spectra were recorded at pH 7.5.

blue. This is expected because of the smaller π-electron system and was also observed for other heme proteins.[27] More importantly, where the position of the Soret bands of unliganded ferriheme and ferroheme forms suggests the presence of the His-on case, the Soret band position of $NP7_{sym}[Fe^{II}–NO]$ corresponds to a 5c species, i.e., His-off.

DISCUSSION

Fe^{II}−His Bond Breakage Observed in NP7. The breakage of the Fe^{II}−His bond in the case of the unliganded *wt* NP7[Fe^{II}] and NP7(E27Q)[Fe^{II}] at neutral pH is a remarkable case in the sense that the Fe^{II}−His60 bond is so weak that it breaks, at least in part, already in the 5cHS state, which is then in equilibrium with the 5cHS state with a water on according to Scheme 1. Table 3 summarizes the results of this study with respect to the stability of the Fe^{II}−His bond in NPs at pH 7.5. To the best of our knowledge, the heme c_n (or heme *x*) in the cytochrome b_6f complex is the only naturally occurring example of a heme without a direct iron−side chain ligation, i.e., a 5c water complex.[75,c] The only other example of a His-liganded ferroheme with a His-on:His-off ratio similar to those of NP7 and NP7(E27Q) is AXCP and a couple of proximal and distal site mutants thereof.[76] Therefore, in this study, we address the factors that contribute to the destabilization of this interaction in NP7[Fe^{II}]. Unfortunately, for NP7, an experimental structure is currently not available; however, because of the high degree of amino acid sequence identity with NP2 (62%) and the absence of residue shifts in the sequence alignment, a highly reliable homology model of NP7 is available.[14]

Table 3. Summary of the Coordination Geometry Observed in Ferroheme NPs and NP Mutants at pH 5.5 and 7.5

	coordination of the proximal His			
	Fe^{II}		Fe^{II}−NO	
protein	pH 5.5	pH 7.5	pH 5.5	pH 7.5
*wt*NP7[a]	off	on/off	off	off(/on)
wt NP4[18 a]	on	on	on	on
NP7(E27V)[a]	on	on	on(/off)	on(/off)
NP7(E27Q)[a]	off	on/off	off	off
NP2(V24E)[a]	on	on	off	off
NP4(D70A)[a]	on	on	on	on
$NP7_{sym}$[a]		on		off
NP2(D1A)[8]			off	on
NP2(D1A/D29A)[8]			off	off(/on)
NP2(D1A/D36A)[8]			off	off(/on)

[a]This work.

Figure 9 illustrates the proximal site arrangement in NP7 in comparison to NP4 by representing the residues involved by the van der Waals radii of the respective atoms. It is obvious that the arrangement of the residues in the neighborhood of the proximal His60 in NP7 is very dense versus the spatial arrangement of Glu27, Phe43, and His60 compared to the arrangement in NP4 with the much smaller residues Val25, Ala41, and His58.[d] This suggests that the polar and bulky Glu27 cannot orient differently and mediates a certain tension via Phe43 to the proximal His60. In agreement with this hypothesis, the displacement of Glu27 in NP7, i.e., NP7(E27V), retrieves the heme coordination whereas the sterically similar Gln, i.e., NP7(E27Q), shows a behavior similar to that of the *wt*, indicating that the size rather than the charge of Glu27 is responsible for the effects described herein.

The reverse insertion of Glu into NP2, i.e., NP2(V24E), is not sufficient for the destabilization of the Fe^{II}−His bond because the Phe residue, mediating the tension between Glu27 and $His_{proximal}$ in NP7, is missing in NP2(V24E), which has a Ser40 instead. However, the Fe^{II}−His bond in NP2(V24E)-[Fe^{II}] breaks completely upon NO binding (Table 3). The negative *trans* effect of NO decreases the affinity of axial N-donor ligands due to a competition of the π^* orbital of NO and the σ orbital of the N-donor for the d_{z^2} orbital of iron. Thus, the presence of Glu24 in NP2(V24E) creates enough tension for the Fe^{II}−His labilization so that together with the electronic weakening of the NO the proximal bond is broken. These effects may be summarized by Scheme 4 in which the

dx.doi.org/10.1021/bi201073t | *Biochemistry* 2011, 50, 8559–8575

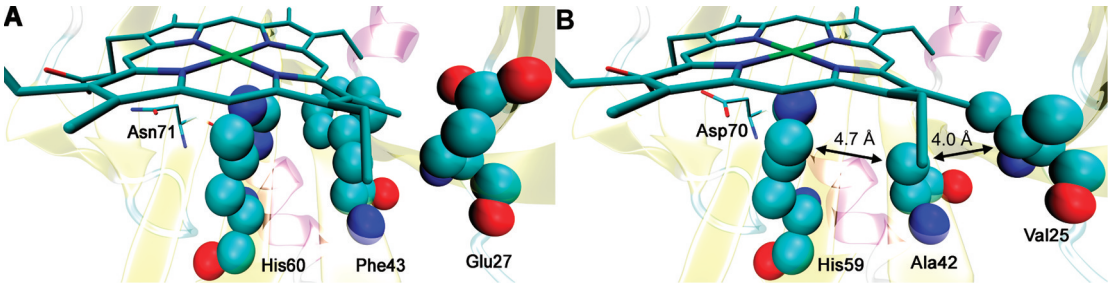

Figure 9. Representation of the spatial arrangement of the proximal heme site in (A) NP7 (homology model[14]) and (B) NP4 (PDB entry 1NP4). Residues Glu27, Phe43, and His60 (A) and Val25, Phe41, and His58 (B) are displayed in their van der Waals radii. In both structures, the heme is displayed in the **A** configuration (compare to Scheme 3). This figure was created with VMD version 1.8.7[111] and rendered with POV-Ray version 3.62 (http://www.povray.org/).

Scheme 4. Tentative Scheme of the Forces Directed to the Heme Cofactor and the Proximal His in NP7 and NP2(V24E) in Comparison to the Situation in Standard Nitrophorins[a]

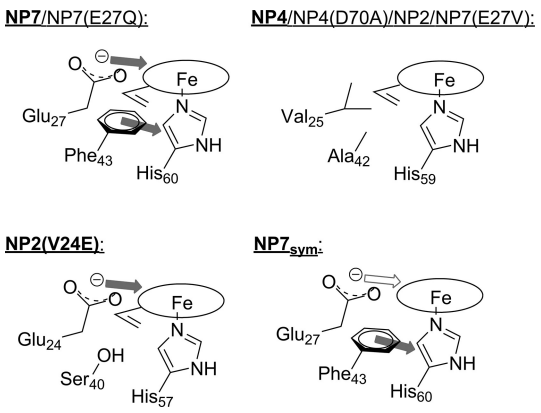

[a]The amino acid numberings correspond to the proteins in bold.

tension created on the Fe^{II}–$His_{proximal}$ bond in NP7 and NP7(E27Q) is depicted as two potential forces indicated by arrows: (i) mediation through Phe43 as described previously and (ii) directly onto the heme plane. In NP2(V24E), the mediation through Phe does not exist, but some tension remains. In contrast, in NP4, NP2, NP7(E27V), and others, no such mechanism exists.

It was previously reported that Glu27 plays a crucial role in the heme properties in NP7, in particular with respect to the orientation of the heme plane inside the pocket,[31,50] which already indicated the very dense situation inside the heme pocket of NP7 (compare to Figure 9). In contrast to NP7, all other NPs exhibit Val24 or -25 (NP2 and -3 or NP1 and -4, respectively) instead. Insertion of the Glu residue into NP2, i.e., NP2(V24E), reverses the heme orientation from **B** to **A** (compare to Scheme 3).[31,50] In contrast, insertion of Val into NP7, i.e., NP7(E27V), reverses the heme orientation from **A** to **B**. In this work, it was shown that both NP7(E27V) and NP7(E27V)[Fe^{II}–NO] do not labilize the Fe^{II}–His60 bond, whereas NP2(V24E)[Fe^{II}–NO] breaks the Fe^{II}–His57 bond. Therefore, the question of the extent that the heme orientation may be involved in His–Fe bond breakage arises.

The insertion of a symmetric heme (compare to Scheme 3) into NP7 shows that the Fe^{II}–His60 bond is indeed preserved in the unliganded situation, demonstrating that the absence of the vinyl group in $NP7_{sym}$ provides enough space for a better fitting into the heme pocket; thus, at least some of the tension from the proximal iron bond is released. On the other hand, $NP7[Fe^{II}–NO]_{sym}$ is a His-off species and, therefore, behaves very much like NP2(V24E). In this case, the force on the $His_{proximal}$ is mediated through Phe43, and a relaxation in the Glu27–heme arrangement is obtained. Furthermore, the influence of the heme vinyl(s) on Fe^{II}–His bond stability demonstrates that the heme orientation matters for the heme properties.

Comparison of NP–NO Five-Coordination with the Behavior of Other Heme Proteins. The molecular mechanisms involved in the biological production, distribution, and sensing of the mammalian signaling molecule NO are currently being investigated. A major key player is the ferroheme protein sGC, which is activated upon coordination of NO to the heme iron and subsequently produces the second-messenger cGMP.[21,77,78] The signal of the NO coordination is mediated through the breakage of the proximal Fe^{II}–His bond as a consequence of the strong negative *trans* effect of NO.[21,79] The resulting conformational change is the trigger for the increase in the level of cGMP formation. However, loss of 6c at ferrohemes upon NO binding occurs rarely in His-coordinated heme proteins, which is in contrast to ferroheme model complexes in which the weak N-base ligands are typically released upon NO binding (K_{eq} = 10–50 M^{-1}).[79] Thus, the entropy gained by the formation of the protein–heme complex compensates for the small free energy of the Fe^{II}–His coordination in most heme protein cases, but what then determines if a Fe^{II}–His bond upon NO binding to a heme inside a protein pocket is broken?

Unfortunately, the structure of the heme domain of sGC is not known, so that structure–function relationships are vague and require comparison with those of proteins with similar features. Furthermore, the binding of NO to sGC may not include only the simple two-step mechanism of (i) NO binding and (ii) His release; it is a matter of debate that by a yet unknown mechanism NO may bind to the proximal iron site according to Scheme 5.[e] While many His-ligated heme proteins

Scheme 5. Mechanism of the Binding of NO to Ferroheme sGC

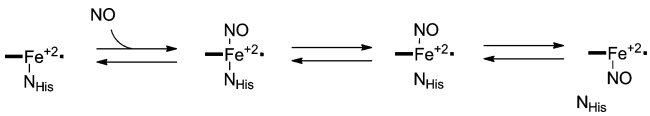

form a 5c Fe^{II}–NO complex only at fairly low pH (e.g., cytochrome *c* at pH 2.0[80] or Mb–NO at pH 4[81]), there are a

dx.doi.org/10.1021/bi201073t | *Biochemistry* 2011, 50, 8559–8575

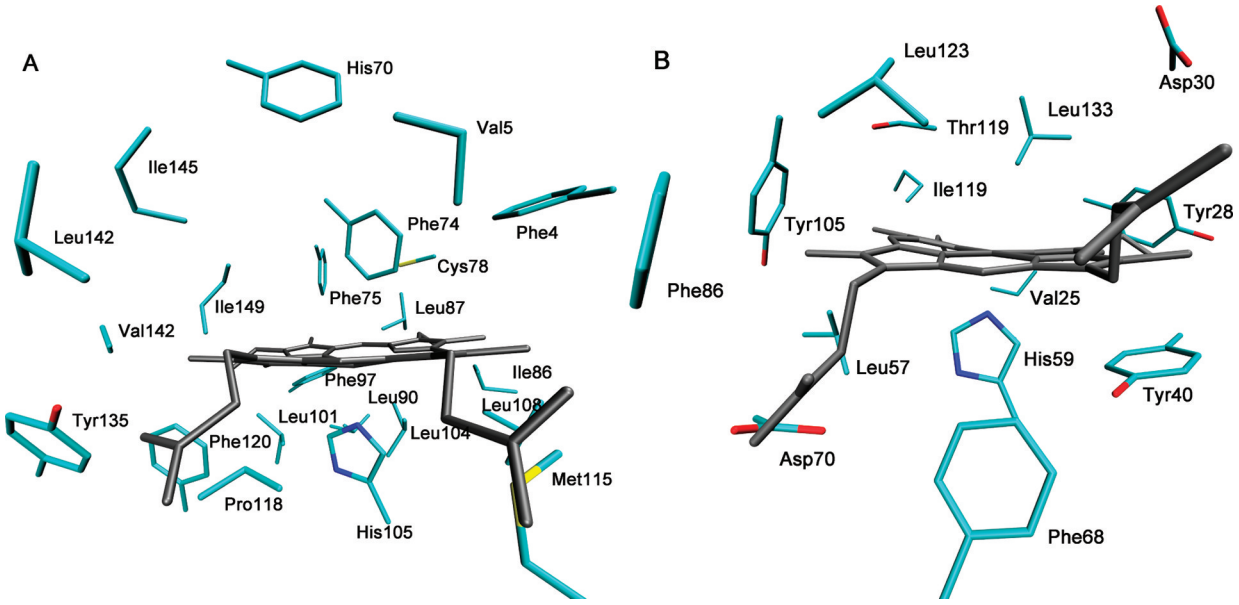

Figure 10. (A) Heme pocket of sGC in comparison with that of (B) NP4. For human sGC, a homology model was used. For NP4, the X-ray structure from PDB entry 1NP4 was used. Figures were prepared with VMD version 1.8.7[111] and rendered with POV-Ray version 3.62 (http://www.povray.org/).

few examples of proteins that break the His N^{τ}–Fe^{II} bond even at approximately neutral pH. To the best of our knowledge, the few examples of non-sGC proteins include CooA, CLOCK PAS-A, the H-NOX domains of *T. tengcongensis*,[82] and the cytochrome *c*′ compounds from various species.[83−85] In particular, the cytochrome *c*′ proteins, originating from bacteria with yet uncertain function, have been studied in the past as models for sGC, and a great advantage is the availability of crystallographic structures of the protein from *A. xylosoxidans*, often termed AXCP.[86] Insights came also from the study of human serum albumin (HSA) and the proximal His deletion mutant H93G of sperm whale Mb [Mb(H93G)] in a complex with ImH, which have been used as model proteins.[87] [A surprisingly different case is heme b_3 of nitric oxide reductase (NoR) that appears His-off in the Fe^{III} state and establishes the Fe–His bond upon reduction to Fe^{II} or NO binding to Fe^{III}.[88]]

On the basis of the results obtained by spectroscopic and crystallographic investigations, the His N^{τ}–Fe^{II} bond weakening in sGC and sGC model proteins was attributed to effects inside the proximal and distal heme pocket. On the distal site, a stabilization of the NO complex by the heme pocket residues was proposed. For example, in Mb the distal His64 residue is able to form an H-bond with NO coordinated to the heme Fe^{II}. However, investigations of the Mb(H64L) and Mb(H64I) mutants by vibrational spectroscopy in combination with DFT calculations revealed a weak interaction of the His–N···N–O bond.[89]

On the proximal site, the influence of certain residues has also been considered. A recent extensive crystallographic and spectroscopic investigation of AXCP and mutant proteins of Arg124 revealed a major contribution of this residue to the affinity and orientation of NO. However, Arg124 forms an H-bond to the proximal NO and stabilizes it, so that the contribution to $His_{proximal}$ at present cannot be estimated. It is also surprising that the large variety of mutants that have been created, i.e., AXCP(R124E), AXCP(R124F), AXCP(R124K), and AXCP(R124Q), exhibit only minor alterations in the NO binding behavior compared to that of the *wt* protein, and that only AXCP(R124A) keep the NO at the distal site.

Recently, an energy-optimized homology model of the human sGC heme domain based on *Ns*H-NOX (PDB entry 2O09)[90] was reported.[91,f] Comparison of the distal heme pockets of sGC with those of NP4 (Figure 10) indicates only aliphatic and aromatic side chains in the vicinity of the heme pocket, in both cases rather densely packed. In contrast, AXCP reveals the Arg124 residue that is able to H-bond to N^{τ} of the proximal His120.[86] Furthermore, it forms an H-bond to NO when the 5c complex at the distal side is formed and, therefore, stabilizes this complex. Whereas such a residue is missing in both sGC and NPs, the latter exhibits a $His_{proximal}$ N^{τ}···water···Asp/Asn network. In NP4, His59 forms an H-bond to the side chain of Asp70 via a water, i.e., His59 H···water···Asp70. However, removal of Asp70 [NP4(D70A)] did not lead to a significant change in the spectroscopic features; in particular, the His-on:His-off ratio was not affected. Thus, it can be concluded that the respective H-bond is not responsible for the stabilization of the Fe^{II}–His bond. It should be noted that, whereas in NP1 Asp70 is also present, in NP2 it is represented by Asn68.[g] However, in both proteins, the Fe^{II}–His bond does not break upon NO binding.[8,33] Inspection of the sGC model structure drew our attention to Asp102 in the case of sGC, which is also present in the *Ns*H-NOX structure. Like in the NPs, $His_{proximal}$ N^{τ} is coordinated to Asp102 via a water; thus, the arrangement likely exists in sGC. On the basis of the data derived from NPs, it can be concluded that the presence or absence of this network may not be important for Fe^{II}–$His_{proximal}$ bond breakage.

ν_{N-O} versus ν_{Fe-N} Anticorrelation in Nitrophorins. Another factor associated with His–Fe bond breakage is the His–Fe bond strength, determination of which can be best estimated by RR spectroscopy where the weak ν_{Fe-His} vibration appears typically in the range of 200–250 cm^{-1}.[92] However, whereas this vibration has been obtained for many proteins, it was, unfortunately, not possible to obtain the vibration with certainty for the nitrophorins even when the excitation wavelength was

dx.doi.org/10.1021/bi201073t | *Biochemistry* 2011, 50, 8559–8575

shifted to 441.6 nm, which typically enhances this mode. Such difficulty was also reported for other heme proteins, for example, CLOCK PAS-A.[69] However, in a comparative study of AXCP and RCCP, it has been recently pointed out that the Fe–$His_{proximal}$ bond strength may not play such a critical role in bond breaking.[65]

Backdonation of the Fe^{II} d_π electrons to the NO π^* orbital is the reason for the negative correlation between the ν_{Fe-N} and ν_{N-O} vibrations.[55,66,93] The correlation of the 5c adducts is linear with a slope of −0.40, whereas the slope of the correlation of the 6c complexes is −1.0 (developed using heme model compounds).[55,66] Both lines are indicated in the plot in Figure 11 together with the ν_{Fe-N}/ν_{N-O} pairs reported herein

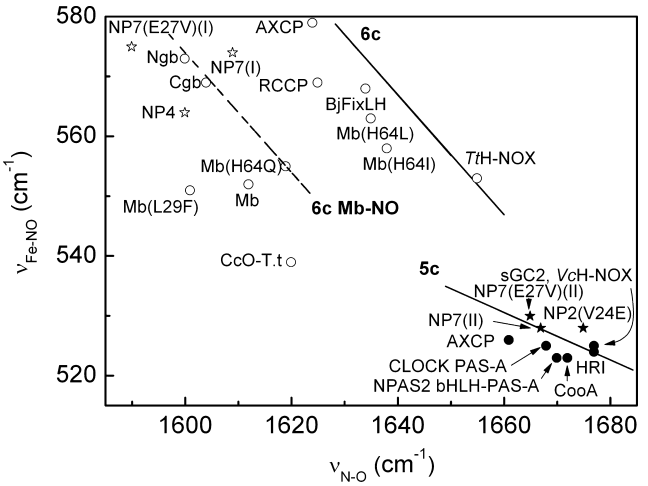

Figure 11. ν_{Fe-NO}/ν_{N-O} correlation plot for the data from heme protein Fe^{II}–NO complexes. The backbonding correlations for the 5c and 6c Fe^{II}–NO porphyrinates and 6c-Mb-NO are from literature.[55,66,93] References for protein complexes are listed in Table 2. The proteins investigated in this study are denoted with stars. Other proteins are denoted with circles. 5c NO complexes are denoted with filled symbols, and 6c NO complexes are denoted with empty symbols.

and a selection of ν_{Fe-N}/ν_{N-O} pairs from proteins. The three 5c complexes reported here, NP7[Fe^{II}–NO], NP7(E27V)[Fe^{II}–NO], and NP2(V24E)[Fe^{II}–NO], fall on this line, which is the case for all the 5c proteins identified so far. The amount of structural data in the case of proteins and model compounds is very limited for the 5c complexes. The variation of model hemes is limited to the variation of substituents at the porphyrin core, and it was demonstrated that the metal–ligand backbonding strength correlates well with the electron withdrawing capabilities of the porphyrin core substituent.[66] However, in the protein examples discovered so far, the macrocycle consists of ppIX; thus, variations in the backbonding must derive from (i) the ligand environment and/or (ii) the heme deformation. However, the only example, to the best of our knowledge, of a 5c protein complexed X-ray structure is reported for AXCP and a number of its mutants.[94] Unfortunately, characterization of the vibrational modes of the Fe–N–O moiety has only been reported for *wt* AXCP. Furthermore, although the proteins fall generally well on the linear correlation, among the heme proteins reported, AXCP is something of an outlier with unusually weak Fe–N and N–O bonds, a fact also reflected in the long Fe–N (2.04 Å) and N–O (1.17 Å) distances (PDB entry 1E85).[86] For comparison, in [Fe(TPP)(NO)] (TPP is 5,10,15,20-tetraphenyl-21*H*,23*H*-porphyrin), the distances are as follows: 1.717 Å for Fe–N and 1.122 Å for N–O.[95] The latter is also characterized by bond angle ∠(Fe–N–O) of 149.2°, which is in good agreement with the {FeNO}^{7} electronic structure, whereas in AXCP, ∠(Fe–N–O) = 125°, which can be attributed to a negative charge density on the NO ligand. In AXCP, the nearby Arg124 was attributed to a particular role in the stabilization of the NO complex through the positive charge on the guanidine group (Arg124 N^ω–NO distance of 3.8 Å).[86] However, comparison of the X-ray structures shows that the Fe–NO bond strongly depends on the charge of residue 124, i.e., Fe–NO distance between 1.81 and 1.93 Å with polar side chain Glu124, Lys124, or Gln124, but 1.73 or 1.75 Å with Phe124 or Ala124, respectively.[94] A similar trend in bond distance was observed for the 6c NO complexes of Mb and its distal site mutant Mb(H64L) based on the ν_{Fe-N} increase (see Figure 11).[75] In contrast, the 5c components of NP7(E27V) and NP7 fit well to the line but are located at the upper end, which reflects greater backbonding character as compared to, for example, that of CooA or sGC. It cannot currently be determined if the NO in 5c NP complexes remains bound to the distal side or moves, like in AXCP (compare Scheme 5), upon loss of the Fe–His bond to the proximal side. A characteristic of the NP distal side is the presence of many aliphatic side chains, which would reduce the polarization of the NO ligand and therefore strengthen Fe–NO backbonding. This interpretation is supported by the fact that the slightly more polar heme pocket of *wt* NP7 has a decreased level of backbonding compared to that of NP7(V24E). On the other hand, the ν_{Fe-N}/ν_{N-O} correlation of NP2(V24E) reflects less backbonding character.

In the case of 6c ferrous NO/His heme proteins, it was previously noticed that the ν_{Fe-N}/ν_{N-O} pairs are much more scattered from the ideal line of model hemes than in the case of the 5c complexes,[55] but also in comparison to those of the well-behaving 6c Fe^{II}–CO complexes.[96] The deviation was attributed to the affection of ∠(Fe–N–O), which should be 142° based on calculations. Hydrogen bonding from His64 in Mb to the NO would potentially strengthen the Fe^{III}–NO^- character,[55] whereas the description of the Fe^{II}–NO center as {FeNO}^{7} provides room to understand the entity as resonances of Fe^{I}–NO^+ ↔ Fe^{II}–NO ↔ Fe^{III}–NO^-.[79] Ngb and Cygb have a similar distal His like Mb, and the distal Cu^+ in CcO creates a similar situation. It was previously determined that many of the 6c NO protein species fall on an alternate line that is parallel to the line derived from model hemes (Figure 11). This was attributed to a stabilization of the Fe^{III}–NO^- mesomeric form by H-bonding of a His residue to N_{NO}, i.e., stabilization of the significant negative charge located at N_{NO}. As a consequence, angle ∠(Fe–N–O) is expected to become significantly less than 140°, which is the ideal case for the Fe^{II}–NO complex, which was confirmed with model hemes.[53,97−99] In the case of Mb, this could not be confirmed crystallographically because, for reasons currently not understood, different Mb[Fe^{II}–NO] crystal structures[100−102] reveal different angles (112–144°)[103] and interatom distances (1.86–2.13 Å Fe–N and 1.17–1.20 Å N–O). On the other hand, this interpretation is supported by the replacement of His64 in Mb with Leu or Ile, which brings the ν_{Fe-N}/ν_{N-O} pair back toward the regular 6c line (see Figure 11).[60,93] However, both experimental and theoretical studies have suggested that the H-bond is likely weak in the case of NO (3–4 kcal/mol), so that the effect seen in vibrational spectroscopy may be more likely due to a polarization of the π/π^* orbitals of the NO.[79,104,105]

As one can see from Figure 11, NP4[Fe^{II}−NO], 6c-NP7[Fe^{II}−NO], and NP7(E27V)[Fe^{II}−NO] fall well on the 6c Mb−NO line. This is interesting because in contrast to the globins, the NPs do not provide a H^+-donating group in the distal pocket. In fact, in the available crystal structures of NP nitrosyls, the closest possible H^+ donor is a water molecule with an O_{water}−O_{NO} distance between 3.7 and 4.1 Å, which should be too week to significantly influence the {FeNO}^{7} entity. Moreover, whereas in the case of NP1[Fe^{II}−NO] the bond angle is indeed 120°, in the high-resolution structures of NP4[Fe^{II}−NO] an angle of 141° or 144° was obtained. (A collection of the available crystal structures of NP nitrosyls is available in Table S1 of the Supporting Information.) Why then do NP4 and NP7 fall on the 6c Mb−NO line?

In this respect, the ferroheme nitrosyl complex of Mb was compared to the oxyMb form,[60,81] which has significant Fe^{III} character, i.e., Fe^{III}−O_2^-, because of an H-bond between His64 and O_2.[106] Studies of the reaction of NP4[Fe^{II}] and NP7[Fe^{II}] with O_2 revealed a very rapid oxidation[34] that can even lead to porphyrin bleaching.[19,32,107] These effects can be best explained by the reaction via the Fe^{III}−O_2^- intermediate. However, while NPs do not provide a H^+ donor in the distal pocket, stabilization of the Fe^{III} state is performed by (i) the localization of numerous carboxylate side chains[8] near the heme pocket and (ii) ruffling of the macrocycle induced by the pocket architecture,[9] which is reflected in the low reduction potentials of the NPs.[6,14] Thus, whereas in the case of oxyMb the Fe^{III} character is induced to the complex upon O_2 binding, the tendency for Fe^{III} formation is an immanent character of NP hemes. However, although this effect is induced for both proteins by different mechanisms, the Fe^{III} character in the {FeNO}^{7} complexes of both proteins may be induced by the same mechanisms as in the O_2 complexes; this may explain why both proteins have a strengthened Fe−N_{NO} bond and thus fall on the 6c Mb−NO line. It is interesting to note that the NP7(E27V)[Fe^{II}−NO]/NP7[Fe^{II}−NO] pair behaves like the Mb[Fe^{II}−NO]/Mb(H64L/I)[Fe^{II}−NO] pair with respect to the large change in ν_{Fe-N} (−19 cm^{-1} vs −23 cm^{-1}), thus reflecting a similar trend in the affection of the Fe^{II}−N_{NO} bond. It should be mentioned that recently the usual interpretation of the lower of the two isotopically sensitive Raman bands of ferroheme nitrosyls as an Fe−N stretch vibration was called into question using nuclear resonance vibrational spectroscopy (NRVS).[79,105] According to these studies, the band may rather reflect the δ_{Fe-N-O} bending vibration and, therefore, reflect both bond angles and bond lengths, which may account for the bad anticorrelation observed in the case of the ferroheme nitrosyls.

In summary, the results obtained in this study reveal the strong tension that the steric demand of neighboring side chains can place on a proximal His−Fe bond in ferroheme proteins. The results are summarized in Scheme 5. Thus, in the case of the very dense arrangement in the heme pocket of NP7, the Glu27 residue, but also Gln27 in NP7(E27Q), together with Phe43 puts a strain on the proximal His, which is responsible for bond breakage. This is indicated by the exchange of Glu27 with Val, which abolishes this behavior. In addition, Glu27 also puts strain on the heme cofactor mediated through the heme vinyls, so that even in the absence of the Phe, insertion of the Glu residue can force the Fe−His bond breakage, as shown with NP2(V24E)[Fe^{II}−NO]. Similarly, removal of the heme vinyls in NP7, i.e., $NP7_{sym}$, breaks the bond more easily than NP7(E27V) does, but $NP7_{sym}$ is more stable than *wt* NP7. Hence, the proteins of this study may be arranged as follows with respect to Fe^{II}−$His_{proximal}$ stability: NP7 ≈ NP7(E27Q) < NP2(V24E) ≈ $NP7_{sym}$ < NP7(E27V) < NP4 ≈ NP4(D70A). By analogy, in the discussion of the question of why the Fe^{II}−$His_{proximal}$ bond breaks in the case of sGC, the steric tension may have been underestimated so far. This study shows that this effect in combination with others, the most important of which certainly is the negative *trans* effect of NO, can play an important role in understanding sGC function.

■ ASSOCIATED CONTENT

Ⓢ Supporting Information

Amino acid sequence alignment of the *R. prolixus* nitrophorins (Figure S1), absorbance spectra of free heme (Figure S2), and summary of the geometry of the Fe−N−O entity in crystal structures of nitrosyl complexes of nitrophorins (Table S1). This material is available free of charge via the Internet at http://pubs.acs.org.

■ AUTHOR INFORMATION

Corresponding Author

*Telephone: +49 (0)208 306 3671. Fax: +49 (0)208 306 3951. E-mail: mknipp@mpi-muelheim.mpg.de.

Funding

This work was financially supported by the Max Planck Society (MPG) and by the Deutsche Forschungsgemeinschaft (DFG), Grants KN 951/1-1 and -2 (to M.K.).

■ ACKNOWLEDGMENTS

The technical assistance of Johanna J. Taing, Robin L. Kosinsky, Jan Hanis, and Marion Stapper is gratefully acknowledged. Dr. Xiangshi Tan, Department of Chemistry and Institutes of Biomedical Sciences, Fudan University, Shanghai (China) is acknowledged for providing the coordination files of the homology model of the sGC heme domain.

■ ABBREVIATIONS

4c, four-coordinate; 5c, five-coordinate; 6c, six-coordinate; AXCP, cytochrome *c*′ from *A. xylosoxidans*; CcO, cytochrome *c* oxidase; CooA, CO oxidation activator protein; Cygb, cytoglobin; cyt *c*′, cytochrome *c*′; DEA/NO, diethylammonium 2-(*N*,*N*-diethylamino)diazenolate-2-oxide; $GS^{15}NO$, *S*-[^{15}N]-nitrosoglutathione; Hb, hemoglobin; HO-1, heme oxygenase 1; HS, high-spin; IS, intermediate-spin; LS, low-spin; MALDI, matrix-assisted laser desorption ionization; Mb, myoglobin; MOPS, 3-(*N*-morpholino)propanesulfonic acid; Ngb, neuroglobin; NOX, nitrogen- and oxygen-sensing; NP, nitrophorin; $NP7_{sym}$, NP7 reconstituted with the "symmetric heme" 2,4-dimethyldeuterohemin; ppIX, protoporphyrin IX; RCCP, cytochrome *c*′ from *R. capsulatus*; TOF, time-of-flight; sGC, soluble guanylate cyclase; SHE, standard hydrogen electrode; TPP, 5,10,15,20-tetraphenyl-21*H*,23*H*-porphyrin; *wt*, wild-type.

ADDITIONAL NOTES

[a]In the presence of Cu^I, GSNO releases NO according to the equation 2GS−NO → GS−SG + 2NO.

[b]This phenomenon was observed in many heme *b* proteins and is often termed heme rotational disorder.

[c]The function of heme c_n is not known. The iron is coordinated by a water or OH^-, which is H-bonded to an Asp side chain.[1]

[d]It should be noted that at present there is no experimental structure of NP7 published. However, a very reliable homology model was built on the basis of the sequence identity with the crystal structure of NP2 (62%). The alignment of the NP2 and NP7 sequences does not have any gaps. The highly similar backbone structure in combination with the compactness of the structure of the heme pocket strongly suggests a very similar local arrangement of the side chains.
[e]At present, it is not possible to decide if the NO binds to the distal or to the proximal iron site of the 5c ferrous NPs.
[f]The coordination file of this model was kindly provided to us by X. Tan, Department of Chemistry and Institutes of Biomedical Sciences, Fudan University, Shanghai, China.
[g]The different numbering of the residues of the different NPs is due to shifts that originate from the sequence alignment (see Figure S1 of the Supporting Information).

REFERENCES

(1) Kurisu, G., Zhang, H., Smith, J. L., and Cramer, W. A. (2003) Structure of the cytochrome b_6f complex of oxygenic photosynthesis: Tuning the cavity. *Science 302*, 1009−1014.
(2) Ribeiro, J.M. C., and Francischetti, I. M. B. (2003) Role of arthropode saliva in blood feeding: Sialome and post-sialome perspectives. *Annu. Rev. Entomol. 48*, 73−88.
(3) Ignarro, L. J. (1990) Biosynthesis and metabolism of endothelium-derived nitric oxide. *Annu. Rev. Pharmacol. Toxicol. 30*, 535−560.
(4) Soares, A. C., Carvalho-Tavares, J., Gontijo, N. d. F., dos Santos, V. C., Teixeira, M. M., and Pereira, M. H. (2006) Salivation pattern of *Rhodnius prolixus* (Reduviidae; Triatominae) in mouse skin. *J. Insect Physiol. 52*, 468−472.
(5) Weichsel, A., Andersen, J. F., Champagne, D. E., Walker, F. A., and Montfort, W. R. (1998) Crystal structures of a nitric oxide transport protein from a blood-sucking insect. *Nat. Struct. Biol. 5*, 304−309.
(6) Walker, F. A. (2005) Nitric oxide interaction with insect nitrophorins and thoughts on the electron configuration of the $\{FeNO\}^6$ complex. *J. Inorg. Biochem. 99*, 216−236.
(7) Hoshino, M., Maeda, M., Konishi, R., Seki, H., and Ford, P. C. (1996) Studies on the reaction mechanism for reductive nitrosylation for ferrihemoproteins in buffer solutions. *J. Am. Chem. Soc. 118*, 5702−5707.
(8) Berry, R. E., Shokhirev, M. N., Ho, A. Y. W., Yang, F., Shokhireva, T. K., Zhang, H., Weichsel, A., Montfort, W. R., and Walker, F. A. (2009) Effect of mutation of carboxyl side-cahin amino acids near the heme on the midpoint potentials and ligand binding constants of nitrophorin 2 and its NO, histamine, and imidazole complexes. *J. Am. Chem. Soc. 131*, 2313−2327.
(9) Shokhireva, T. K., Berry, R. E., Uno, E., Balfour, C. A., Zhang, H., and Walker, F. A. (2003) Electrochemical and NMR spectroscopic studies of distal pocket mutants of nitrophorin 2: Stability, structure, and dynamics of axial ligand complexes. *Proc. Natl. Acad. Sci. U.S.A. 100*, 3778−3783.
(10) Ding, X. D., Weichsel, A., Andersen, J. F., Shokhireva, T. K., Balfour, C., Pierik, A. J., Averill, B. A., Montfort, W. R., and Walker, F. A. (1999) Nitric oxide binding to the ferri- and ferroheme states of nitrophorin 1, a reversible NO-binding heme protein from the saliva of the blood-sucking insect, *Rhodnius prolixus*. *J. Am. Chem. Soc. 121*, 128−138.
(11) Enemark, J. H., and Feltham, R. D. (1974) Principles of structure, bonding, and reactivity for metal nitrosyl complexes. *Coord. Chem. Rev. 13*, 339−406.
(12) Berry, R. E., Ding, X. D., Shokhireva, T. K., Weichsel, A., Montfort, W. R., and Walker, F. A. (2004) Axial ligand complexes of the *Rhodnius* nitrophorins: Reduction potentials, binding constants, EPR spectra, and structures of the 4-iodopyrazole and imidazole complexes of NP4. *J. Biol. Inorg. Chem. 9*, 135−144.
(13) Berry, R. E., Shokhireva, T. K., Filippov, I., Shokhirev, M. N., Zhang, H., and Walker, F. A. (2007) The effect of the N-terminus on heme cavity structure, ligand equilibrium and rate constants and reduction potentials of nitrophorin 2 from *Rhodnius prolixus*. *Biochemistry 46*, 6830−6843.
(14) Knipp, M., Yang, F., Berry, R. E., Zhang, H., Shokhirev, M. N., and Walker, F. A. (2007) Spectroscopic and functional characterization of nitrophorin 7 from the blood-feeding insect *Rhodnius prolixus* reveals an important role of its isoform-specific N-terminus for proper protein function. *Biochemistry 46*, 13254−13268.
(15) Traylor, T. G., and Sharma, V. S. (1992) Why NO? *Biochemistry 31*, 2847−2849.
(16) Nienhaus, K., Maes, E. M., Weichsel, A., Montfort, W. R., and Nienhaus, G. U. (2004) Structural dynamics controls nitric oxide affinity in nitrophorin 4. *J. Biol. Chem. 279*, 39401−39407.
(17) Benabbas, A., Ye, X., Kubo, M., Zhang, Z., Maes, E. M., Montfort, W. R., and Champion, P. M. (2010) Ultrafast dynamics of diatomic ligand binding to nitrophorin 4. *J. Am. Chem. Soc. 132*, 2811−2820.
(18) Maes, E. M., Roberts, S. A., Weichsel, A., and Montfort, W. R. (2005) Ultrahigh resolution structures of nitrophorin 4: Heme distortion in ferrous CO and NO complexes. *Biochemistry 44*, 12690−12699.
(19) Ribeiro, J. M. C. (1996) Salivary thiol oxidase activity of *Rhodnius prolixus*. *Insect Biochem. Mol. Biol. 26*, 899−905.
(20) Daff, S. (2010) NO synthase: Structures and mechanisms. *Nitric Oxide 23*, 1−11.
(21) Poulos, T. L. (2006) Soluble guanylate cyclase. *Curr. Opin. Struct. Biol. 16*, 736−743.
(22) Gladwin, M. T., Grubina, R., and Doyle, M. P. (2009) The new chemical biology of nitrite reactions with hemoglobin: R-state catalysis, oxidative denitrosylation, and nitrite reductase/anhydrase. *Acc. Chem. Res. 42*, 157−167.
(23) Basu, S., Grubina, R., Huang, J., Conradie, J., Huang, Z., Jeffers, A., Jiang, A., He, X., Azarov, I., Seibert, R., Mehta, A., Patel, R., King, B. S., Hogg, N., Ghosh, A., Gladwin, M. T., and Kim-Shapiro, D. B. (2007) Cataclytic generation of N_2O_3 by the concerted nitrite reductase and anhydrase activity of hemoglobin. *Nat. Chem. Biol. 3*, 785−794.
(24) Creutz, C., and Sutin, N. (1973) Reduction of ferricytochrome *c* by dithionite ion: Electron transfer by parralel adjacent and remote pathways. *Proc. Natl. Acad. Sci. U.S.A. 70*, 1701−1703.
(25) Knipp, M., Braun, O., and Vašák, M. (2005) Searching for DDAH inhibitors: *S*-Nitroso-L-homocysteine is a chemical lead. *J. Am. Chem. Soc. 127*, 2372−2373.
(26) Braun, O., Knipp, M., Chesnov, S., and Vašák, M. (2007) Specific reactions of *S*-nitrosothiols with cysteine hydrolases: A comparative study between dimethylargininase-1 and CTP synthetase. *Protein Sci. 16*, 1522−1534.
(27) Neya, S., Suzuki, M., Hoshino, T., Ode, H., Imai, K., Komatsu, T., Ikezaki, A., Nakamura, M., Furutani, Y., and Kandori, H. (2010) Molecular insights into intrinsic heme distortion in ligand binding in hemoprotein. *Biochemistry 49*, 5642−5650.
(28) Hintz, M. J., and Peterson, J. A. (1980) The kinetics of reduction of cytochrome $P\text{-}450_{cam}$ by the dithionite anion monomer. *J. Biol. Chem. 255*, 7317−7325.
(29) Wang, W., and Malcolm, B. A. (1999) Two-stage PCR protocol allowing introduction of multiple mutations, deletions and insertions using QuikChange Site-Directed Mutagenesis. *BioTechniques 26*, 680−682.
(30) Knipp, M., Zhang, H., Berry, R. E., and Walker, F. A. (2007) Overexpression in *Escherichia coli* and functional reconstitution of the liposome binding ferriheme protein nitrophorin 7 from the blood sucking bug *Rhodnius prolixus*. *Protein Expression Purif. 54*, 183−191.
(31) Yang, F., Zhang, H., and Knipp, M. (2009) A one-residue switch reverses the orientation of a heme *b* cofactor. Investigations on the ferriheme NO transporters nitrophorin 2 and 7 from the blood-feeding insect *Rhodnius prolixus*. *Biochemistry 48*, 235−241.

(32) Knipp, M., Taing, J. J., and He, C. (2011) Reduction of the lipocalin type heme containing protein nitrophorin: Sensitivity of the fold-stabilizing cysteine disulfides toward routine heme-iron reduction. *J. Inorg. Biochem.*, DOI: doi: 10.1016/j.jinorgbio.2011.07.009.
(33) Andersen, J. F., Ding, X. D., Balfour, C., Shokhireva, T. K., Champagne, D. E., Walker, F. A., and Montfort, W. R. (2000) Kinetics and equilibria in ligand binding by nitrophorins 1−4: Evidence for stabilization of a nitric oxide-ferriheme complex through a ligand-induced conformational trap. *Biochemistry 39*, 10118−10131.
(34) Knipp, M., and He, C. (2011) Nitrophorins: Nitrite disproportionation reaction and other novel functionalities of insect heme-based nitric oxide transport proteins. *IUBMB Life 63*, 304−312.
(35) Palaniappan, V., and Bocian, D. F. (1994) Acid-induced transformations of myoglobin. Characterization of a new equilibrium heme-pocket intermediate. *Biochemistry 33*, 14264−14274.
(36) Tang, Q., Kalsbeck, W. A., Olson, J. S., and Bocian, D. F. (1998) Disruption of the heme iron-proximal histidine bond requires unfolding of deoxymyoglobin. *Biochemistry 37*, 7047−7056.
(37) Spiro, T. G., and Li, X.-Y. (1988) Resonance Raman spectroscopy of metalloporphyrins. In *Resonance Raman Spectra of Heme and Metalloproteins* (Spiro, T. G., Ed.) 1st ed., pp 1−38, John Wiley & Sons, New York.
(38) Spiro, T. G., and Czernuszewicz, R. S. (2000) Resonance Raman Spectroscopy. In *Physical Methods in Bioinorganic Chemistry: Spectroscopy and Magnetism* (Que, L., Jr., Ed.) 1st ed., pp 59−119, UniversityScience Books, Sausalito, CA.
(39) Maes, E. M., Walker, F. A., Montfort, W. R., and Czernuszewicz, R. S. (2001) Resonance Raman spectroscopic study of nitrophorin 1, a nitric oxide-binding heme protein from *Rhodnius prolixus*, and its nitrosyl and cyano adducts. *J. Am. Chem. Soc. 123*, 1164−1172.
(40) Kincaid, J. R. (2000) Resonance Raman spectra of heme proteins and model compounds. In *The Porphyrin Handbook* (Kadish, K. M., Smith, K. M., and Guilard, R., Eds.) 1st ed., pp 225−291, Academic Press, San Diego.
(41) Andersson, L. A., Mylrajan, M., Sullivan, E. P. Jr., and Strauss, S. H. (1989) Modeling low-pH hemoproteins. *J. Biol. Chem. 264*, 19099−19102.
(42) Kitagawa, T., Kyogoku, Y., Iizuka, T., and Saito, M. I. (1976) Nature of the iron-ligand bond in ferrous low spin hemoproteins studied by resonance Raman scattering. *J. Am. Chem. Soc. 98*, 5169−5173.
(43) Spiro, T. G., Stong, J. D., and Stein, P. (1979) Porphyrin core expansion and doming in heme proteins. New evidence from resonance Raman spectra of six-coordinate high-spin iron(III) hemes. *J. Am. Chem. Soc. 101*, 2648−2655.
(44) Sage, J. T., Morikis, D., and Champion, P. M. (1991) Spectroscopic studies of myoglobin at low pH: Heme structure and ligation. *Biochemistry 30*, 1227−1237.
(45) Vetter, S. W., Terentis, A. C., Orsborne, R. L., Dawson, J. H., and Goodin, D. B. (2009) Replacement of the axial histidine heme ligand with cysteine in nitrophorin 1: Spectroscopic and crystallographic characterization. *J. Inorg. Biol. Chem. 14*, 179−191.
(46) He, C., and Knipp, M. (2009) Formation of nitric oxide from nitrite by the ferriheme *b* protein nitrophorin 7. *J. Am. Chem. Soc. 131*, 12042−12043.
(47) Sun, J., Loehr, T. M., Wilks, A., and Ortiz de Montellano, P. R. (1994) Identification of histidine 25 as the heme ligand in human liver heme oxygenase. *Biochemistry 33*, 13734−13740.
(48) Kitagawa, T., Ozaki, Y., Kyogoku, Y., and Horio, T. (1977) Resonance Raman study of the pH-dependent and detergent-induced structural alterations in the heme moiety of *Rhodospirillum rubrum* cytochrome *c*′. *Biochim. Biophys. Acta 495*, 1−11.
(49) Hobbs, J. D., Larsen, R. W., Meyer, T. E., Hazzard, J. H., Cusanovich, M. A., and Ondrias, M. R. (1990) Resonance Raman characterization of *Chromatium vinosum* cytochrom *c*′. Effect of pH and comparison of equilibrium and photolyzed cabron monoxide species. *Biochemistry 29*, 4166−4174.
(50) Yang, F., Knipp, M., Shokhireva, T. K., Berry, R. E., Zhang, H., and Walker, F. A. (2009) A ^{1}H and ^{13}C NMR spectroscopic study of the ferriheme resonances of three low-spin complexes of wild-type nitrophorin 2 and nitrophorin2(V24E) as a function of pH. *J. Biol. Inorg. Chem. 14*, 1077−1095.
(51) Decatur, S. M., Franzen, S., DePillis, G. D., Dyer, R. B., Woodruff, W. H., and Boxer, S. G. (1996) *Trans* effect in nitric oxide binding to myoglobin cavity mutant H93G. *Biochemistry 35*, 4939−4944.
(52) Ford, P. C. (2010) Reactions of NO and nitrite with heme models and proteins. *Inorg. Chem. 49*, 6226−6239.
(53) Praneeth, V. K. K., Näther, C., Peters, G., and Lehnert, N. (2006) Spectroscopic properties and electronic structure of five- and six-coordinate iron(II) porphyrin NO complexes: Effect of the axial N-donor ligand. *Inorg. Chem. 45*, 2795−2811.
(54) Scheidt, W. R., and Ellison, M. K. (1999) The synthetic and structural chemistry of heme derivatives with nitric oxide ligands. *Acc. Chem. Res. 32*, 350−359.
(55) Ibrahim, M., Xu, C., and Spiro, T. G. (2006) Differential sensing of protein influences by NO and CO vibrations in heme addcuts. *J. Am. Chem. Soc. 128*, 16834−16845.
(56) Reynolds, M.F., Parks, R. B., Burstyn, J. N., Shelver, D., Thorsteinsson, M. V., Kerby, R. L., Roberts, G. P., Vogel, K. M., and Spiro, T. G. (2000) Electronic absorption, EPR, and resonance Raman spectroscopy of CooA, a CO-sensing transcription activator from *R. rubrum*, reveals a five-coordinate NO-heme. *Biochemistry 39*, 388−396.
(57) Tomita, T., Ogura, T., Tsuyama, S., Imai, Y., and Kitagawa, T. (1997) Effects of GTP on bound nitric oxide of soluble guanylate cyclase probed by resonance Raman spectroscopy. *Biochemistry 36*, 10155−10160.
(58) Mukaiyama, Y., Uchida, T., Sato, E., Sasaki, A., Sato, Y., Igarashi, J., Kurokawa, H., Sagami, I., Kitagawa, T., and Shimizu, T. (2006) Spectroscopic and DNA-binding characterization of the isolated heme-bound basic helix-loop-helix-PAS-A domain of neuronal PAS protein 2 (NPAS2), a transcription activator associated with circadian rythms. *FEBS J. 273*, 2528−2539.
(59) Schade, D., Kotthaus, J., and Clement, B. (2010) Modulating the NO generating system from a medicinal chemistry perspective: Current trends and therapeutic options in cardiovascular disease. *Pharmacol. Ther. 126*, 279−300.
(60) Tomita, T., Hirota, S., Ogura, T., Olson, J. S., and Kitagawa, T. (1999) Resonance raman investigation of Fe-N-O structure of nitrosylheme in myoglobin and its mutants. *J. Phys. Chem. B 103*, 7044−7054.
(61) Sawai, H., Makino, M., Mizutani, Y., Ohta, T., Sugimoto, H., Uno, T., Kawada, N., Yoshizato, K., Kitagawa, T., and Shiro, Y. (2005) Structural characterization of the proximal and distal histidine environment of cytoglobin and neuroglobin. *Biochemistry 44*, 13257−13265.
(62) Lukat-Rodgers, G. S., and Rodgers, K. R. (1997) Characterization of ferrous FixL-nitric oxide adducts by resonance raman spectroscopy. *Biochemistry 36*, 4178−4187.
(63) Tomita, T., Gonzalez, G., Chang, A. L., Ikeda-Saito, M., and Gilles-Gonzalez, M. A. (2002) A comparative resonance Raman analysis of heme-binding PAS domains: Heme iron coordination structures of the *Bj*FixL, *Ax*PDEA1, *Ec*Dos, and *Mt*Dos proteins. *Biochemistry 41*, 4819−4826.
(64) Andrew, C. R., George, S. J., Lawson, D. M., and Eady, R. R. (2002) Six- to five-coordinate heme-nitrosyl conversion in cytochrome *c*′ and its releveance to guanylate cyclase. *Biochemistry 41*, 2353−2360.
(65) Andrew, C. R., Kemper, L. J., Busche, T. L., Tiwari, A. M., Kecskes, M. C., Stafford, J. M., Croft, L. C., Lu, S., Moënne-Loccoz, P., Huston, W., Mior, J. W. B., and Eady, R. R. (2005) Accessibility of the distial heme face, rather than Fe-His bond strength, determines the heme-nitrosyl coordination number of cytochromes *c*′: Evidence from spectroscopic studies. *Biochemistry 44*, 8664−8672.
(66) Vogel, K. M., Kozlowski, P. M., Zgierski, M. Z., and Spiro, T. G. (1999) Determinants of the FeXO (X = C, N, O) vibrational frequencies in heme adducts from experiment and density functional theory. *J. Am. Chem. Soc. 121*, 9915−9921.

(67) Deinum, G., Stone, J. R., Babcock, G. T., and Marletta, M. A. (1996) Binding of nitric oxide and carbon monoxide to soluble guanylate cyclase as observed with resonance Raman spectroscopy. *Biochemistry 35*, 1540−1547.
(68) Stone, J. R., and Marletta, M. A. (1994) Soluble guanylate cyclase from bovine lung: Activation with nitric oxide and carbon monoxide and spectral characterization of the ferrous and ferric states. *Biochemistry 33*, 5636−5640.
(69) Lukat-Rodgers, G. S., Correia, C., Botuyan, M. V., Mer, G., and Rodgers, K. R. (2010) Heme-based sensing by the mammalian circadian protein CLOCK. *Inorg. Chem. 49*, 6349−6365.
(70) Vogel, K. M., Hu, S., Spiro, T. G., Dierks, E. A., Yu, A. E., and Burstyn, J. N. (1999) Variable forms of soluble guanylyl cyclase: Protein-ligand interactions and the issue of activation by carbon monoxide. *J. Biol. Inorg. Chem. 4*, 804−813.
(71) Yu, A. E., Hu, S., Spiro, T. G., and Burstyn, J. N. (1994) Resonance Raman Spectroscopy of Soluble Guanylyl Cyclase Reveals Displacement of Distal and Proximal Heme Ligands by NO. *J. Am. Chem. Soc. 116*, 4117−4118.
(72) Shokhireva, T. K., Smith, K. M., Berry, R. E., Shokhirev, N. V., Balfour, C. A., Zhang, H., and Walker, F. A. (2007) Assignment of the ferriheme resonances of the high-spin forms of nitrophorins 1 and 4 by ^{1}H NMR spectroscopy: Comparison to structural data obtained from X-ray crystallography. *Inorg. Chem. 46*, 170−178.
(73) Shokhireva, T. K., Weichsel, A., Smith, K. M., Berry, R. E., Shokhirev, N. V., Balfour, C. A., Zhang, H., Montfort, W. R., and Walker, F. A. (2007) Assignment of the ferriheme resonances of the low-spin complexes of nitrophorins 1 and 4 by ^{1}H and ^{13}C NMR spectroscopy: Comparison to structural data obtained from X-ray crystallography. *Inorg. Chem. 46*, 2041−2056.
(74) Shokhireva, T. K., Berry, R. E., Zhang, H., Shokhirev, M. N., and Walker, F. A. (2008) Assignment of ferriheme resonances for high- and low-spin forms of nitrophorin 3 by ^{1}H and ^{13}C NMR spectroscopy and comparison to nitrophorin 2: Heme pocket structural similarities and differences. *Inorg. Chim. Acta 361*, 925−940.
(75) Baniulis, D., Yamashita, E., Zhang, H., Hasan, S., and Cramer, W. A. (2008) Structure-function of the cytochrome b_6f complex. *Photochem. Photobiol. 84*, 1349−1358.
(76) Barbieri, S., Murphy, L. M., Sawers, R. G., Eady, R. R., and Hasnain, S. S. (2008) Modulation of NO binding to cytochrome *c*′ by distal and proximal haem pocket residues. *J. Biol. Inorg. Chem. 13*, 531−540.
(77) Sharma, V. S., and Madge, D. (1999) Activation of soluble guanylate cyclase by carbon monoxide and nitric oxide: A mechanistic model. *Methods 19*, 494−505.
(78) Hobbs, A. J. (1997) Soluble guanylate cyclase: The forgotten sibling. *Trends Pharmacol. Sci. 18*, 484−491.
(79) Goodrich, L. E., Paulat, F., Praneeth, V. K. K., and Lehnert, N. (2010) Electronic structure of heme-nitrosyls and its significance for nitric oxide reactivity, sensing, transport, and toxicity in biological systems. *Inorg. Chem. 49*, 6293−6316.
(80) Yoshimura, T., and Siuzuki, S. (1988) The pH dependence of the stereochemistry around the heme group in NO-cytochrome *c* (horse heart). *Inorg. Chim. Acta 152*, 241−249.
(81) Duprat, A. F., Traylor, T. G., Wu, G.-Z., Coletta, M., Sharma, V. S., Walda, K. N., and Magde, D. (1995) Myoglobin-NO at low pH: Free four-coordinate heme in the protein pocket. *Biochemistry 34*, 2634−2644.
(82) Pellicena, P., Karow, D. S., Boon, E. M., Marletta, M. A., and Kuriyan, J. (2004) Crystal structure of an oxygen-binding heme domain related to soluble guanylate cyclases. *Proc. Natl. Acad. Sci. U.S.A. 101*, 12854−12859.
(83) Suzuki, S., Yoshimura, T., Nakahara, A., Iwasaki, H., Shidara, S., and Matsubara, T. (1987) Electronic and magnetic circular dichroism spectra of pentacoordinate nitrosylhemes in cytochromes *c*′ from nonphotosynthetic bacteria and their model complexes. *Inorg. Chem. 26*, 1006−1008.
(84) Iwasaki, H., Yoshimura, T., Suzuki, S., and Shidara, S. (1991) Spectral properties of *Achromobacter xylosoxidans* cytochrome *c*′ and their NO complexes. *Biochim. Biophys. Acta 1058*, 79−82.
(85) Yoshimura, T., Fujii, S., Kamada, H., Yamaguchi, K., Suzuki, S., Shidara, S., and Takakuwa, S. (1996) Spectroscopic characterization of nitrosylheme in nitric oxide complexes of ferric and ferrous cytochrome *c*′ from photosynthetic bacteria. *Biochim. Biophys. Acta 1292*, 39−46.
(86) Lawson, D. M., Stevenson, C. E. M., Andrew, C. R., and Eady, R. R. (2000) Unprecedented proximal binding of nitric oxide to heme: Implications for guanylate cyclase. *EMBO J. 19*, 5661−5671.
(87) Kharitonov, V. G., Sharma, V. S., Magde, D., and Koesling, D. (1997) Kinetics of nitric oxide dissociation from five- and six-coordinate nitrosyl hemes and heme proteins, including soluble guanylate cyclase. *Biochemistry 36*, 6814−6818.
(88) Pinakoulaki, E., Gemeinhardt, S., Saraste, M., and Varotsis, C. (2002) Nitric-oxide reductase: Structure and properties of the catalytic site from resonance Raman scattering. *J. Biol. Chem. 277*, 23407−23413.
(89) Xu, C., and Spiro, T. G. (2008) Ambidentate H-bonding by heme-bound NO: Structural and spectral effects of -O versus -N H-bonding. *J. Biol. Inorg. Chem. 13*, 613−621.
(90) Ma, X., Sayed, N., Beuve, A., and van den Akker, F. (2007) NO and CO differentially activate soluble guanylate cyclase via a heme pivot-bend mechanism. *EMBO J. 26*, 578−588.
(91) Zhong, F., Wang, H., Ying, T., Huang, Z.-X., and Tan, X. (2010) Efficient expression of human soluble guanylate cyclase in *Escherichia coli* and its signaling-related interaction with nitric oxide. *Amino Acids 39*, 399−408.
(92) Kitagawa, T. (1988) in *Biological Applications of Raman Spectroscopy* (Spiro, T. G., Ed.) pp 97−131, John Wiley & Sons, New York.
(93) Coyle, C. M., Vogel, K. M., Rush, T. S. III, Kozlowski, P. M., Williams, R., Spiro, T. G., Dou, Y., Ikeda-Saito, M., Olson, J. S., and Zgierski, M. Z. (2003) FeNO structure in distal pocket mutants of myoglobin based on resonance Raman spectroscopy. *Biochemistry 42*, 4896−4903.
(94) Hough, M. A., Antonyuk, S. V., Barbieri, S., Rustage, N., McKay, A. L., Servid, A. E., Eady, R. R., Andrew, C. R., and Hasnain, S. S. (2011) Distal-to-proximal NO conversion in hemoproteins: The role of the proximal pocket. *J. Mol. Biol. 405*, 395−409.
(95) Scheidt, W. R., and Frisse, M. E. (1975) Nitrosylmetalloporphyrins. II. Synthesis and molecular sterochemistry of nitrosyl-$\alpha,\beta,\gamma,\delta$-tetraphenylporphinatoiron(II). *J. Am. Chem. Soc. 97*, 17−21.
(96) Spiro, T. G., and Wasbotten, I. H. (2005) CO as a vibrational probe of heme protein active sites. *J. Inorg. Biochem. 99*, 34−44.
(97) Wyllie, G. R. A., Schulz, C. E., and Scheidt, W. R. (2003) Five- to six-coordination in (nitrosyl)iron(II) porphyrinates: Effects of binding the sixth ligand. *Inorg. Chem. 42*, 5722−5734.
(98) Scheidt, W. R., and Piciulo, P. L. (1976) Nitrosylmetalloporphyrins. III. Synthesis and molecular stereochemistry of nitrosyl-$\alpha,\beta,\gamma,\delta$-tetraphenylporphinato(1-methylimidazole)iron(II). *J. Am. Chem. Soc. 98*, 1913−1919.
(99) Silvernail, N. J., Pavlik, J. W., Noll, B. C., Schulz, C. E., and Scheidt, W. R. (2008) Reversible NO motion in crystaline [Fe(porphy)(1-MeIm)(NO)] derivatives. *Inorg. Chem. 47*, 912−920.
(100) Copeland, D. N., Soares, A. S., West, A. H., and Richter-Addo, G. B. (2006) Crystal structures of the nitrite and nitric oxide complexes of horse heart myoglobin. *J. Inorg. Biochem. 100*, 1413−1425.
(101) Brucker, E. A., Olson, J. S., Ikeda-Saito, M., and Phillips, G. N. Jr. (1998) Nitric oxide myoglobin: Crystal structure and analysis of ligand geometry. *Proteins: Struct., Funct., Genet. 30*, 352−356.
(102) Copeland, D. N., West, A. H., and Richter-Addo, G. B. (2003) Crystal structure of ferrous horse heart myoglobin complexed with nitric oxide and nitrosoethane. *Proteins: Struct., Funct., Genet. 53*, 182−192.
(103) A study of multiple scattering analysis of XAFS data from a frozen solution of Mb[Fe^{II}-NO] yielded 150°: Rich, A. M.,

Armstrong, R. S., Ellis, P. J., and Lay, P. A. (1998) Determination of the Fe−Ligand Bond Lengths and Fe−N−O bond angles in horse heart ferric and ferrous nitrosylmyoglobin using multiple-scattering XAFS analyses. *J. Am. Chem. Soc. 120*, 10827−10836.

(104) Tangen, E., Savadberg, A., and Ghosh, A. (2005) Toward modeling H-NOX domains: A DFT study of heme-NO complexes as hydrogen bond acceptors. *Inorg. Chem. 44*, 7802−7805.

(105) Lehnert, N., Sage, J. T., Silvernail, N., Scheidt, W. R., Alp, E. E., Sturhahn, W., and Zhao, J. (2010) Oriented single-crystal nuclear resonance vibration spectroscopy of [Fe(TPP)(MI)(NO)]: Quantitative assessment of the *trans* effect of NO. *Inorg. Chem. 49*, 7197−7215.

(106) Sigfridsson, E., and Ryde, U. (1999) On the significance of hydrogen bonds for the discrimination between CO and O_2 by myoglobin. *J. Biol. Inorg. Chem. 4*, 99−110.

(107) Ribeiro, J.M. C. (1998) *Rhodnius prolixus* salivary nitrophorins display heme-peroxidase activity. *Insect Biochem. Mol. Biol. 28*, 1051−1057.

(108) Karow, D. S., Pan, D., Tran, R., Pellicena, P., Presley, A., Mathies, R. A., and Marletta, M. A. (2004) Spectroscopic characterization of the soluble guanylate cyclase-like heme domains from *Vibrio cholerae* and *Thermoanaerobacter tengcongensis*. *Biochemistry 43*, 10203−10211.

(109) Mukaiyama, Y., Uchida, T., Sato, E., Sasaki, A., Sato, Y., Igarashi, J., Kurikawa, H., Sagami, I., Kitagawa, T., and Shimizu, T. (2006) Spectroscopic and DNA-binding characterozation of the isolated heme-bound basic helix-loop-helix-PAS-A domain of neuronal PAS protein 2 (NPAS2), a transcription activator protein associated with circadian rythms. *FEBS J. 273*, 2528−2539.

(110) Igarashi, J., Sato, A., Kitagawa, T., Yoshimura, T., Yamauchi, S., Sagami, I., and Shimizu, T. (2004) Activation of heme-regulated eukaryotic initiator factor 2α kinase by nitric oxide is induced by the formation of a five-coordinate NO-heme complex. Optical absorption, electron spin resonance, and resonance Raman spectral studies. *J. Biol. Chem. 279*, 15752−15762.

(111) Humphrey, W., Dalke, A., and Schulten, K. (1996) VMD: Visual Molecular Dynamics. *J. Mol. Graphics 14*, 33−38.